Peroxide-mediated oxidations

Doctoral Thesis

Author(s):
Turrà, Natascia

Publication date:
2013

Permanent link:
https://doi.org/https://doi.org/10.3929/ethz-a-009904699

Diss. ETH No. 21087

PEROXIDE-MEDIATED OXIDATIONS

A dissertation submitted to

ETH ZURICH

for the degree of

DOCTOR OF SCIENCES

presented by

NATASCIA TURRÀ

MSc Chemical and Bioengineering, ETH Zurich

born on December 17, 1983

citizen of Zurich (ZH) and Italy

accepted on the recommendation of

Prof. Dr. Ive Hermans

Prof. Dr. Willem H. Koppenol

2013

"The person who follows the crowd

will usually get no further than the crowd.

The one who walks alone is likely to find himself

in places no one has ever been before."

(anonymous)

ACKNOWLEDGMENT

First of all, I would like to thank Prof. Dr. Ive Hermans for his supervision, guidance, support and the opportunity to complete this doctoral thesis in his group at the Institute for Chemical and Bioengineering (ICB). His research advice, deep knowledge of chemistry and reaction engineering has been a great motivation.

Moreover, I thank Prof. Dr. Willem H. Koppenol for accepting the task of co-examiner and for his proficient review of this work.

Being the second co-worker (and the first chemical engineer) of the Hermans Group, I could not only help in setting up the labs, but also take over part of the responsibility for the students and events. In this regard, I want to acknowledge the technical staff at ETH, in particular Andreas Dutly for his advice with the GCs and the great time during the lab courses, Roland Walker, Jean-Pierre Mächler, Roland Mäder, Philippe Trüssel, Markus Küpfer and Urs Krebs for their immense help and patience adapting the equipment for my research, Ján Kovacovic for his assistance in the high pressure lab, Erol Dedeoglu for computer-related problems and Max Haueter for his support in secretariate questions. Very special thanks go to Max Wohlwend who was always of help with electronic issues, but also for the inspiring and relaxing KGs and for introducing me to the "Chlaus" family.

I want to thank Bernhard Mayr-Schmölzer for being the first student under my supervision and for assisting with finding the best solution to make the high pressure autoclaves inert for the autoxidation experiments. Andrea Blanco Acuña's enthusiastic commitment during her Master thesis was extremely helpful.

To this point, I want to thank all the group members Eyal Spier, Martin Schümperli, Christof Aellig, Philipp Mania, Sabrina Conrad, Patrick Wolf, Dr. Ceri Hammond and Dr. Camila Marchetti Maroneze for the great atmosphere and the many funny moments during these years. Many thanks go to Dr. Ulrich Neuenschwander, the first Hermans Group alumnus, who always helped me during his time in our group and who still assists me with his computational knowhow. The Baiker Group was my first research family, and part of it is still present in my life. I thank Dr. Daniel M. Meier for his never-ending support starting at my research project and throughout the years, Dr. Cecilia Mondelli and Dr. Gianluca Santarossa for their friendship and Dr. Ronny Wirz for his help during my Master thesis and his advice with the IR equipment.

I am profoundly thankful to all my friends who encouraged me during these doctoral studies, especially Milena Wild who shared my undergraduate studies and who expected the conclusion of this thesis passionately; Michele Furlotti for his power to make me laugh at any time; Claudia Russo and Nicole Bernaschina for being constantly present with good advices.

Finally, I want to thank my family for having made me stronger at any occasion. Special thanks go to my brother Alessandro who has always been there for me and somehow followed my steps to ETH, and to my "sisters" Assunta and Rita Geracitano for the inspiring talks and the cheerful messages from far south in Italy… Last, but not least, I thank my fiancé Stefano Cordelli for his love and encouragement during the last years. He turned me into a better person.

TABLE OF CONTENTS

PEROXIDE-MEDIATED OXIDATIONS

SUMMARY

Oxyfunctionalizing organic molecules is an important value creating step throughout the entire chemical value chain. Being the products of such reactions more reactive than the parent compound, the major challenge in this field is the prevention of side reactions and/or the consecutive overoxidation. Despite its importance, a fundamental understanding of the intrinsic chemistry, and the subsequent design of a tailored engineering environment, is often missing. Industrial oxidation processes are indeed to a large extent based on empirical knowhow. In chapter 1, the current state-of-the-art and the strategies for the industrial oxidation of cyclohexane are summarized.

Explosive gas mixtures are formed when hydrocarbon vapors and oxygen meet within certain limits. In chapter 2, the experimental set-up used to study aerobic oxidations under high pressure conditions is presented, together with appropriate safety measures to reduce the explosion probability and to protect personnel.

The reactor wall can have a significant effect on the observed activity and selectivity during lab-scale studies of oxidation reactions. This makes it difficult to record the background activity and selectivity of autoxidations. Fenton-type decomposition of peroxides *via* metal ions coming from the reactor wall not only reduces the efficiency, but it can also cause safety issues, when not anticipated, as it forms oxygen which can build explosive gas mixtures in the reactor. Scale-up problems may also arise since the reactor surface-to-volume ratio is inversely proportional to the reactor radius; large scale industrial

reactors are thus much less subjective to wall effects than small lab reactors. In order to reduce the reactivity of the reactor wall, and/or to prevent metal ion leaching, different construction materials have been tested for their inertness towards deperoxidation; Polyether Ether Ketone (PEEK) has shown to have the lowest activity and was thus chosen as the most adequate material for the autoclave inserts.

The homolytic cleavage of peroxide bonds, leading to the formation of free radicals, plays an important role in the (spontaneous) oxidation of a wide variety of hydrocarbons in presence of oxygen. Such aerobic oxidations can be desired (*e.g.*, for industrially applied autoxidations) or undesired (*e.g.*, food deterioration). In chapter 3, experimental and computational evidence for a molecule-induced homolytic dissociation mechanism between alkyl peroxide and compounds featuring weakly bonded H-atoms such as (di)unsaturated hydrocarbons is provided; substrates which are susceptible to autoxidation are not only reacting very rapidly with radicals, they are also faster in generating radicals *via* the described mechanism.

Chapter 4 focuses on the Co^{II}/Co^{III}-induced decomposition of hydroperoxides (ROOH), referred to as deperoxidation. In the first step of the Fenton-type reaction cycle, alkoxyl radicals ($RO^{\bullet}$) and Co^{III}-OH species are generated upon the reaction of the Co^{II} ion with ROOH. The catalytic cycle is closed upon the regeneration of the Co^{II} ion through the reaction of the Co^{III}-OH species with a second ROOH molecule, thus producing one equivalent of the peroxyl radicals ($ROO^{\bullet}$). The deperoxidation of *tert*-butyl hydroperoxide by dissolved cobalt(II) acetylacetonate is studied by using UV/Vis spectroscopy *in situ* with a noninteracting solvent, namely, cyclohexane. Kinetic information extracted from experiments, together with quantum-chemical calculations, led to new mechanistic hypotheses. Even under anaerobic conditions, the Fenton-type cycle initiates a radical chain destruction of ROOH propagated by both alkoxyl and peroxyl radicals. This chain mechanism rationalizes the high deperoxidation rates, which are directly proportional to the cobalt concentration. At higher cobalt concentrations, a net decrease of the reaction rate is observed. A clear inhibition mechanism could not be proposed, however, it is hypothesized that cobalt in a higher reaction order, forming dimers or oligomers, must be involved. For this reason, we decided to test a heterogeneous catalyst which obviously cannot undergo such dimerization being immobilized on a support.

The high pressure aerobic oxidation of cyclohexane was thus studied at 130 °C in the presence of a Co/SiO_2 catalyst, synthesized by flame spray pyrolysis. Characterization of the material indicates that at low Co loadings, Co^{II} is predominantly present as tetrahedral species, whereas at higher loadings also small amounts of octahedral species can be found at the surface of the agglomerated nanoparticles. Catalytic experiments in chapter 5 demonstrate high activity, causing a complete *in situ* deperoxidation of the intermediate cyclohexyl hydroperoxide, similar to autoxidations carried out with the homogeneous catalyst Co(II) acetylacetonate. These results were independent of the Co loading of the particles. No rate deceleration was observed at higher cobalt concentrations. Hot separation and catalyst recycle tests corroborate the heterogeneous nature of the catalyst.

During these doctoral studies some steps could be made towards a better understanding of the complex autoxidation mechanism. Different approaches led to interesting insights. Several future research topics are proposed in the outlook to further characterize and verify the various mechanistic cycles.

ZUSAMMENFASSUNG

Der chemische Ausdruck Oxidation, der in dieser Arbeit benutzt wird, bezieht sich ausschliesslich auf die Sauerstoffaufnahme durch organisches Material, und wird auch Oxifunktionalisierung genannt. Diese ist ein äusserst wichtiger wertschaffender Schritt in der gesamten chemischen Wertschöpfungskette. Die grösste Herausforderung innerhalb dieses Forschungsgebietes ist die Vermeidung von Nebenreaktionen und/oder von Über-oxidationen, da die dabei entstehenden Produkte reaktiver sind als deren Edukte. Trotz ihrer Wichtigkeit, fehlt oft ein grundlegendes Verständnis der intrinsischen Chemie, und folglich der Planung eines bedarfsgerechten technischen Umfeldes. Tatsächlich basieren industrielle Oxidationsprozesse vorwiegend auf empirischem Wissen. Kapitel 1 fasst den gegenwärtigen Stand von Wissenschaft und Technik und die verschiedenen industriellen Verfahren zur Cyclohexanoxidation zusammen.

Explosive Gasgemische entstehen, wenn Kohlenwasserstoffdämpfe mit Sauerstoff innerhalb von bestimmten Grenzwerten in Kontakt kommen. In Kapitel 2 wird der Versuchs-aufbau, der zur Forschung aerobischer Oxidationen unter Hochdruckbedingungen benutzt wurde, zusammen mit den angebrachten Sicherheitsmassnahmen zur Reduktion der Explosionsgefahr und zum Schutz des Personals vorgestellt.

Die Reaktorwand kann die beobachtete Aktivität und Selektivität während der Untersuchung der Oxidationen im Labormassstab erheblich beeinflussen. Dies erschwert die Bestimmung des Autoxidationsnulleffekts unter thermischen Bedingungen. Die Spaltung der

Peroxide durch Metallionen aus der Reaktorwand verringert nicht nur die Effizienz, sondern kann bei falscher Einschätzung erhebliche Sicherheitsprobleme verursachen, da diese Reaktion zur Sauerstoffbildung und folglich zu möglichen explosiven Gasgemische im Reaktor führen kann. Die Übertragung vom Labor auf eine technische Grossanlage wird dadurch ebenfalls erschwert, da sich das Oberflächen-zu-Volumen-Verhältnis anti-proportional zum Reaktorradius verhält. Demnach reagieren Reaktoren im industriellen Massstab viel weniger sensitiv auf Wandeffekte als kleine Laborreaktoren. Verschiedene Werkstoffe wurden auf ihre Inertheit gegenüber Peroxidspaltung getestet, um die Eigenreaktivität des Reaktors und die Auslaugung der Metallionen zu unterbinden; Poly-etheretherketon (PEEK) zeigte die niedrigste Aktivität und wurde deswegen als das geeignetste Material für die Autoklaveneinsätze gewählt.

Die homolytische Spaltung von Peroxidbindungen, die zur Bildung zweier freier Radikale führt, spielt eine wesentliche Rolle in der (spontanen) Oxidation von einer Vielzahl an Kohlenwasserstoffen unter Anwesenheit von Sauerstoff. Solche aerobischen Oxidationen können erwünscht (z.B. bei industriell angewandten Autoxidationen) oder unerwünscht (z.B. Lebensmittelfäulnis) sein. Kapitel 3 liefert experimentelle und rechnergestützte Belege für einen molekülinduzierten homolytischen Dissoziationsmechanismus zwischen Alkyl-peroxiden und Verbindungen, die schwach gebundene H-Atome aufweisen, wie zum Beispiel (zweifach) ungesättigte Kohlenwasserstoffe. Substrate, die für Autoxidationen anfälllig sind, reagieren nicht nur sehr schnell mit Radikalen, sie sind auch rascher in der Bildung von Radikalen mittels des beschriebenen Mechanismus.

In Kapitel 4 wird auf die Co^{II}/Co^{III}-induzierte Spaltung von Hydroperoxiden (ROOH), die auch als Deperoxidation bekannt ist, eingegangen. Im ersten Schritt des Reaktionszyklus nach Fenton werden Alkoxylradikale ($RO^{\bullet}$) und Co^{III}-OH Spezies durch die Reaktion von Co^{II} Ionen mit ROOH erzeugt. Der katalytische Zyklus wird durch die Wiederfreisetzung des Co^{II} Ions durch die Reaktion der Co^{III}-OH Spezies mit einem zweiten ROOH Molekül geschlossen, wobei ein Äquivalent an Peroxylradikalen entsteht ($ROO^{\bullet}$). Die Deperoxidation von *tert*-Butylhydroperoxid durch in Cyclohexan gelöstes Kobalt(II)acetylacetonat wurde *in situ* unter Verwendung von UV/Vis Spektroskopie untersucht. Die kinetischen Informationen, die aus den Experimenten gewonnen wurden, führten zusammen mit quantenchemischen Berechnungen zu neuen mechanistischen Hypothesen. Selbst unter anaeroben Bedingungen iniziiert der Fentonzyklus eine Radikalkettenspaltung der ROOH Moleküle, die durch Alkoxyl- und Peroxylradikale propagiert wird. Dieser Kettenmechanismus rationalisiert die hohe Deperoxidationsgeschwindigkeit, die direkt proportional zur Kobaltkonzentration ist. Eine deutliche Abnahme der Reaktionsgeschwindigkeit wurde bei hohen Kobaltkonzentrationen beobachtet. Obwohl kein eindeutiger Inhibierungsmechanismus vorgeschlagen werden konnte, wird angenommen, dass das Kobalt in einer höheren Reaktionsordnung, d.h. durch die Bildung von dimeren oder oligomeren Spezies, eine entscheidende Rolle spielen muss. Aus diesem Grund wurde im Folgenden ein heterogener Katalysator getestet, da für diesen Dimerisierungen und Oligomerisierungen ausgeschlossen werden können, weil die Metallionen auf der Oberfläche eines Trägermaterials immobilisiert sind.

Die aerobische Oxidation von Cyclohexan wurde hierfür bei 130 °C und unter hohem Druck in Anwesenheit eines Co/SiO_2 Katalysators, der durch Flammenspraypyrolyse (FSP) synthetisiert wurde, untersucht. Die Charakterisierung des Materials zeigte, dass die Co^{II} Spezies bei niedrigem Kobaltgehalt vorwiegend als tetraedrische Spezies vorhanden sind, während bei höherem Gehalt auch oktaedrische Spezies auf der Oberfläche der agglomerierten Nanopartikel zu finden sind. Die in Kapitel 5 dargestellten katalytischen Experimente ergaben hohe Aktivitäten, die eine vollständige *in situ* Deperoxidation des Zwischenprodukts Cyclohexylhydroperoxid zur Folge haben und somit ähnliche Ergebnisse zu den Autoxidationsexperimenten mit homogenem Co(II)-Katalysator liefern. Diese Resultate waren unabhängig vom Kobaltgehalt der Nanopartikel. Auch bei höheren Kobaltkonzentrationen wurde keine Geschwindigkeitsverminderung beobachtet. Die

Abtrennung des Katalysators im Verlauf der Reaktion (hot filtration test) sowie Tests zur Wiederverwertung des Katalysators bestätigten dessen heterogene Eigenschaft.

Während dieser Doktorarbeit konnten einige Schritte in Richtung eines besseren Verständnisses des äussert komplexen Autoxidationsmechanismus gemacht werden. Unterschiedliche Ansätze führten zu interessanten Erkenntnissen. Einige mögliche Forschungsthemen, die zur weiteren Charakterisierung und Überprüfung verschiedener mechanistischer Zyklen führen könnten, werden im Ausblick vorgeschlagen.

1

INTRODUCTION

Oxyfunctionalizing organic molecules is an important value creating step throughout the entire chemical value chain. The major challenge in this field is the prevention of side reactions and/or the consecutive overoxidation of the desired products. Despite its importance, a fundamental understanding of the intrinsic chemistry, and the subsequent design of a tailored engineering environment, is often missing. Industrial oxidation processes are indeed to a large extent based on empirical knowhow. In this chapter, we summarize the current state-of-the-art.

1.1 Oxidations

The chemical term oxidation used in this work refers to the uptake of oxygen by organic material and is also referred to as oxyfunctionalization.[1] Oxidations are highly exothermic reactions. Under normal conditions, all organic matter exists as metastable intermediates on the way to CO_2 which is the only thermodynamically stable carbon compound at ambient temperature. However, the kinetics of oxidation reactions is unfavoured at low temperatures. Even more problematic is the selective (or partial) oxidation of these hydrocarbons, since oxygenated compounds (*i.e.*, products of such partial oxidations) are usually more susceptible to (over)oxidation.

Oxygen is the cheapest oxidant, because unlike the other known oxidants (*e.g.*, CrO_3, H_2O_2) it does not need to be produced using O_2. Unfortunately, reactions with oxygen are far less selective and require higher investments. This is only worthwhile on a scale exceeding 10^4 - 10^5 t/y, depending on the product.

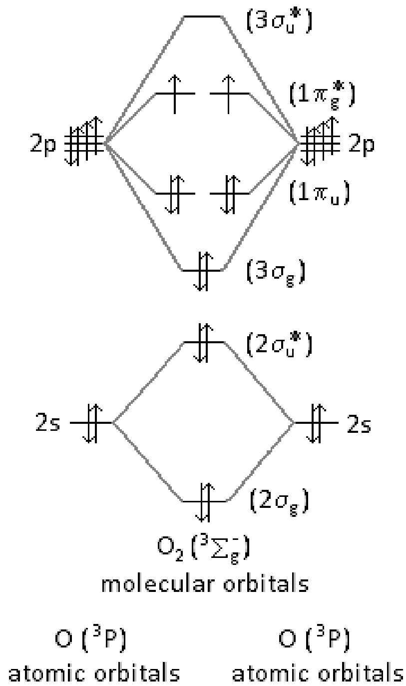

Figure 1-1. Molecular orbitals of ground state triplet oxygen.

Molecular oxygen is one of the few simple molecules whose electronic ground state is triplet ($^{3}\Sigma_{g}^{-}$). As can be seen in Figure 1-1, the molecular orbital $1\pi_{g}^{*}$ is half occupied. Because of this electronic ground state, oxygen has a net electron spin 1 and is paramagnetic. The spin conservation rule (Wigner rule) implies that only transitions between terms of the same spin multiplicity are spin-allowed.[2] Reactions with organic compounds, which usually have singlet electronic ground state, are thus forbidden and hence very slow. Singlet oxygen (*i.e.*, O_2 in an excited state) reacts as a two-electron oxidant and is much more reactive towards diamagnetic substances than triplet O_2.

Oxidations can be divided into homolytic and heterolytic reactions, depending on the nature of the reaction intermediates.[3] In the case of homolytic chemistry, radicals (*e.g.*, peroxyl radicals) are formed as reactive intermediates whereas in heterolytic oxidation reactions, an active oxygen compound (*e.g.*, a peroxy acid or H_2O_2), or a metal ion in a high valence state (*e.g.*, CrO_3), oxidizes the substrate in a two-electron transfer reaction, thereby preventing the formation of radicals. Normally, a stoichiometric amount of the oxidizing compound is used in combination with a catalyst, for instance a complex of Mo^{VI}, V^{V}, or Ti^{IV}. The catalyst can be dissolved homogeneously in a liquid or alternatively be present in solid form.

Unless O_2 is explicitly activated on a catalyst (*e.g.*, a silver surface as for ethylene epoxidation), aerobic oxidations often involve radical chemistry.

1.2 Radical Chain Chemistry

1.2.1 Conventional and Revised Mechanism

If a hydrocarbon is heated in the presence of oxygen, a spontaneous oxidation will take place in which the slow direct reaction is bypassed by a much more efficient radical mechanism (reactions (1-1)-(1-6)). The concept of radical chain reactions was proposed by Bäckström in 1927.[4] In 1939, Criegee and Pilz discovered that the main product of cyclohexene oxidation was allyl hydroperoxide,[5] and Farmer could then propose the first radical chain mechanism of the homolytic oxidation of hydrocarbons.[6]

$$ROOH \rightarrow RO^\bullet + {}^\bullet OH \qquad (1\text{-}1)$$

$$RO^\bullet + RH \rightarrow ROH + R^\bullet \qquad (1\text{-}2)$$

$${}^\bullet OH + RH \rightarrow H_2O + R^\bullet \qquad (1\text{-}3)$$

$$R^\bullet + O_2 \rightarrow ROO^\bullet \qquad (1\text{-}4)$$

$$ROO^\bullet + RH \rightarrow ROOH + R^\bullet \qquad (1\text{-}5)$$

$$ROO^\bullet + ROO^\bullet \rightarrow ROH + Q{=}O + O_2 \qquad (1\text{-}6)$$

This type of oxidation – referred to as autoxidation – is of great industrial importance. Some large-scale examples are: the oxidation of *p*-xylene to terephthalic acid (44×10^6 t/y), synthesis of cyclohexanol and cyclohexanone (6×10^6 t/y, Figure 1-2, see section 1.2.3), and the oxidation of cumene to cumene hydroperoxide (5×10^6 t/y).

Previous work revealed that the actual autoxidation mechanism is insufficiently known. It was for instance assumed that during the liquid phase autoxidation of cyclohexane, the alcohol (ROH) and ketone (Q=O) products are exclusively formed in the termination reaction of two peroxyl radicals ($ROO^\bullet$, reaction (1-6)).[3] However, it is known that the rate of reaction (1-5) is much higher than the rate of reaction (1-6), the ratio being referred to as the chain length ($\nu \geq 10$). This would imply that the yield of ROH and Q=O would be much smaller than the alkyl hydroperoxide (ROOH) yield, in disagreement with the experimental observations (Figure 1-2).

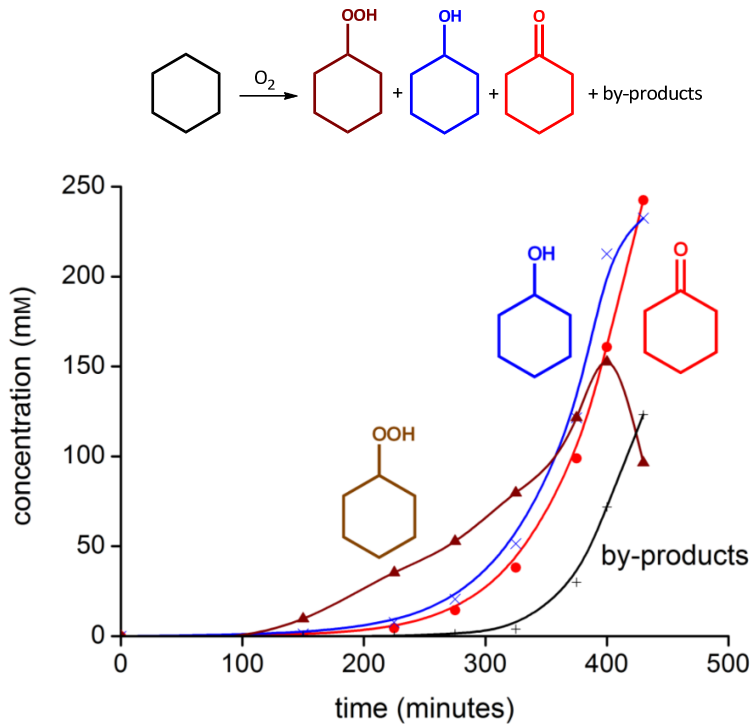

Figure 1-2. Product distribution for the cyclohexane oxidation, showing cyclohexyl hydroperoxide (CyOOH) as the primary product.

Based on a combination of detailed experiments and theoretical calculations,[7, 8] it was proposed that there exists a much faster alcohol and ketone channel than known so far. This overlooked mechanism starts with the rapid abstraction of a weakly bonded αH-atom from the primary hydroperoxide product. The resulting radical ($R_{-\alpha H}{}^{\bullet}OOH$) is not stable and promptly dissociates to Q=O and $^{\bullet}OH$, immediately explaining the ketone product (reaction (1-7)).[9]

$$ROO^{\bullet} + ROOH \rightarrow ROOH + Q{=}O + {}^{\bullet}OH \qquad (1\text{-}7)$$

The hydroxyl radical co-produced in reaction (1-7) will rapidly abstract an H-atom from the ubiquitous alkane molecules surrounding the nascent ROOH + Q=O + $^{\bullet}OH$ products (reaction (1-8), Scheme 1-1). The resulting products can either diffuse away from each other (reaction (1-9)), or undergo cage-reaction (1-10) (Scheme 1-2).

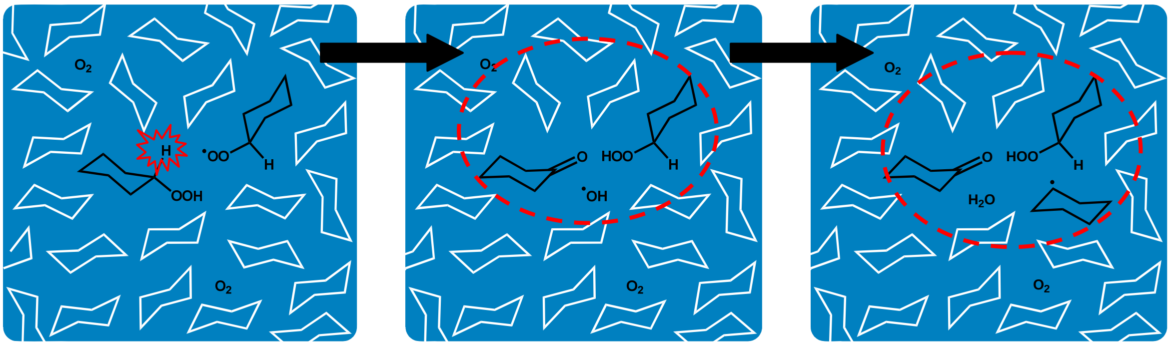

Scheme 1-1. αH-abstraction (reaction (1-7)) and subsequent cage-reaction (1-8) for the cyclohexane autoxidation.[9]

$$\{ROOH + Q{=}O + {}^{\bullet}OH\} + \{RH\}^{cage\text{-}wall} \longrightarrow \{ROOH + R^{\bullet} + Q{=}O + H_2O\}^{cage} \tag{1-8}$$

$$\{ROOH + R^{\bullet} + Q{=}O + H_2O\}^{cage} \longrightarrow ROOH + R^{\bullet} + Q{=}O + H_2O \tag{1-9}$$

$$\{ROOH + R^{\bullet} + Q{=}O + H_2O\}^{cage} \longrightarrow \{RO^{\bullet} + ROH + Q{=}O + H_2O\}^{cage} \tag{1-10}$$

Although the diffusive separation (reaction (1-9)) faces a lower barrier than cage-reaction (1-10), the latter channel can compete, due to the formation of a local hot-spot. This nano-sized hot-spot is generated by the high exothermicity of the previous reaction steps (1-7) and (1-8), generating together approximately 209 kJ mol^{-1}.[8] Kinetic modeling experiments show that in case of cyclohexane, reaction (1-10) accounts for 70% of the reaction flux, in close agreement with the theoretical predictions.[8] More reactive substrates, such as toluene and ethylbenzene, feature cage efficiencies of only 56 and 22%, respectively.[10, 11] For those substrates, the alkyl radicals are more stabilized, leading to a higher barrier for reaction (1-10). In the case of cyclohexane oxidation, the alkoxyl radicals coproduced in cage-reaction (1-10) were found to be responsible for the majority of ring-opened by-products (Scheme 1-3), rather than the overoxidation of cyclohexanone as assumed so far.[12] This hitherto unknown solvent cage effect in radical autoxidations readily explains quantitatively the observed product distributions for a wide range of substrates.

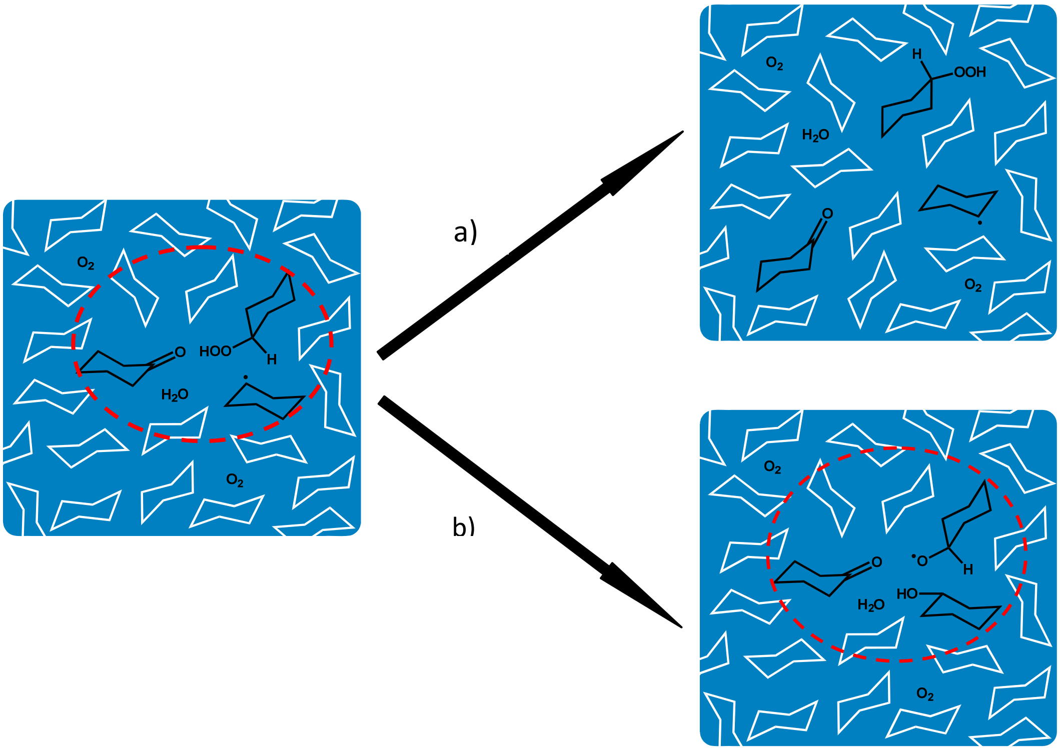

Scheme 1-2. Diffusion (a, reaction (1-9)) versus cage-reaction (b, reaction (1-10)) for the cyclohexane autoxidation.[7]

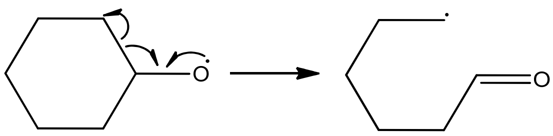

Scheme 1-3. Reaction mechanism responsible for the formation of most ring-opened by-products from alkoxyl radicals ($RO^{\bullet}$).

The role of reaction (1-1) as the dominant initiation mechanism was also questioned. Indeed, this reaction is not only very slow due to its 167 kJ mol^{-1} activation barrier (despite the fact that the reaction is unimolecular), it is also very inefficient in the liquid phase as the nascent radicals will preferably recombine within their solvent cage, rather than to diffuse away from each other and initiate a radical chain.[13] It was shown that the actual initiation mechanism is a bimolecular reaction of the primary hydroperoxide product with either the substrate (*e.g.*, in the case of ethylbenzene), or with one of the reaction products (*e.g.*, cyclohexanone in the case of cyclohexane oxidation).[13] The latter reaction also explains the autocatalytic nature of cyclohexane autoxidation: during the reaction, cyclohexanone is produced which accelerates the initiation mechanism.

1.2.2 Fenton-Type Chemistry

There are two different ways in which autoxidations can be catalyzed: (i) either by accelerating the rate-determining initiation reaction or (ii) *via* the introduction of species which are more efficient chain carriers than peroxyl radicals (catalyzing the propagation, suppressing the termination, *e.g.*, addition of *N*-hydroxyphtalimide; see section 3.1).

Transition metal ions which are able to undergo one-electron redox reactions (*e.g.*, $Co^{II/III}$, $Mn^{II/III}$, $Fe^{II/III}$) are known to accelerate the initiation rate *via* the Fenton mechanism (reactions (1-11) and (1-12)).[7]

$$ROOH + Co^{II} \rightarrow RO^{\bullet} + Co^{III}\text{-}OH \qquad (1\text{-}11)$$

$$ROOH + Co^{III}\text{-}OH \rightarrow ROO^{\bullet} + Co^{II} + H_2O \qquad (1\text{-}12)$$

In presence of such catalytic ions, reactions (1-11) and (1-12) take over the role of $ROO^{\bullet}$ in the destruction of ROOH, leading to an *in situ* deperoxidation.

1.2.3 Industrial Cyclohexane Oxidation

Before World War II, cyclohexanol (CyOH) and cyclohexanone (Q=O) were industrially produced *via* reduction of phenol. In the 1940s, the (transition metal catalyzed) aerobic liquid phase oxidation of cyclohexane was developed and became the most important route.[14] The majority of all Q=O produced is further converted to adipic acid or to cyclohexanone oxime, the precursor of caprolactam. CyOH is used as well for the production of adipic acid, or is further oxidized to Q=O. Both compounds are also used as a solvent, or as starting materials for fine chemicals. KA-oil (*i.e.*, Q=O/CyOH mixture), with a production of 6×10^6 t/y, is thus an extremely important bulk intermediate. Scheme 1-4 shows the CyOH/Q=O value chain.

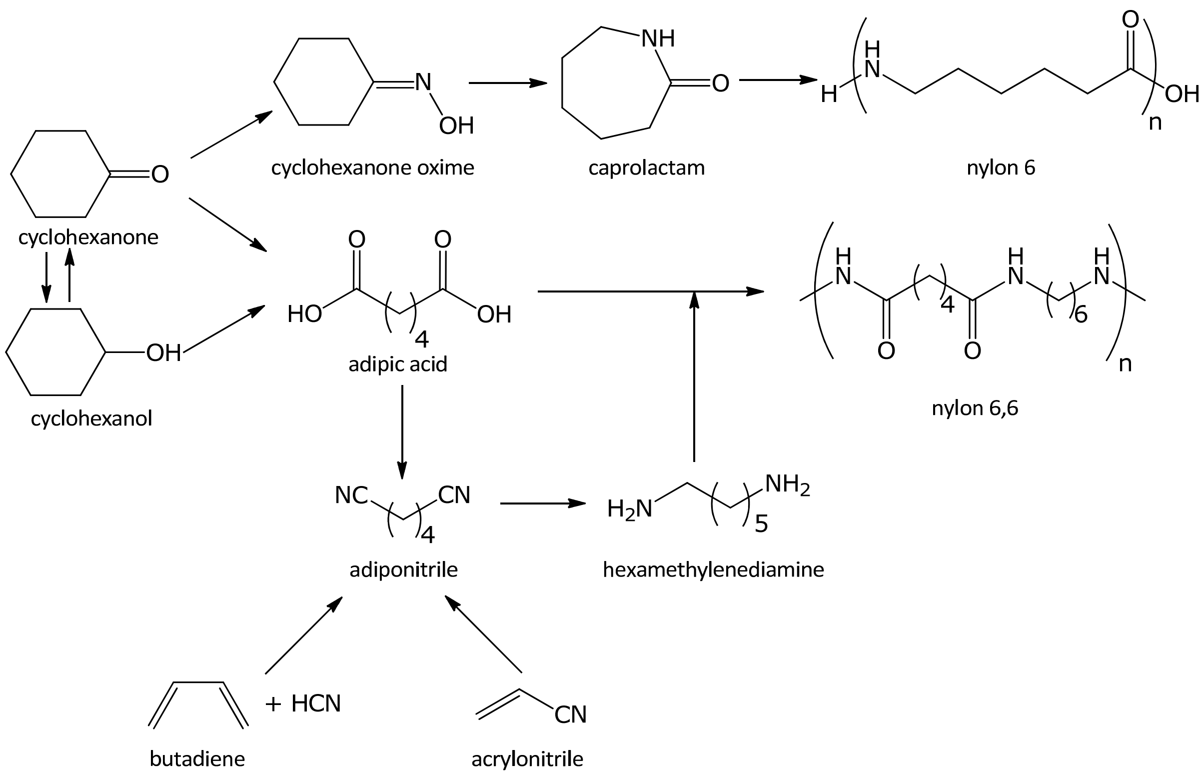

Scheme 1-4. Part of the C_6 value chain: KA-oil as crucial intermediate for the polyamides nylon 6 and nylon 6,6.

Generally, there exist three different strategies for the industrial oxidation of cyclohexane (Scheme 1-5).[1, 3, 15] In a first approach (Scheme 1-5a), cyclohexane is oxidized to a mixture of CyOOH, CyOH and Q=O without a catalyst in a series of agitated reactors at temperatures of 150-180 °C (residence times: 15-60 min). To remove acidic by-products, the product stream leaving the oxidizers is usually washed with water, followed by a deperoxidation of (remaining) CyOOH to additional CyOH and Q=O with a homogeneous cobalt catalyst. In another approach (Scheme 1-5b), small amounts (ppb-range, since the catalyst is not recycled) of transition metal salts (*e.g.*, cobalt(II) 2-ethylhexanoate) are already added to the oxidation reactor (130-150 °C). An extensive work-up of the reaction mixture is required also in this approach (*viz.* deperoxidation and separation). Both processes are limited to a conversion of about 5% and produce KA-oil with an ol:one ratio of about 2-3.

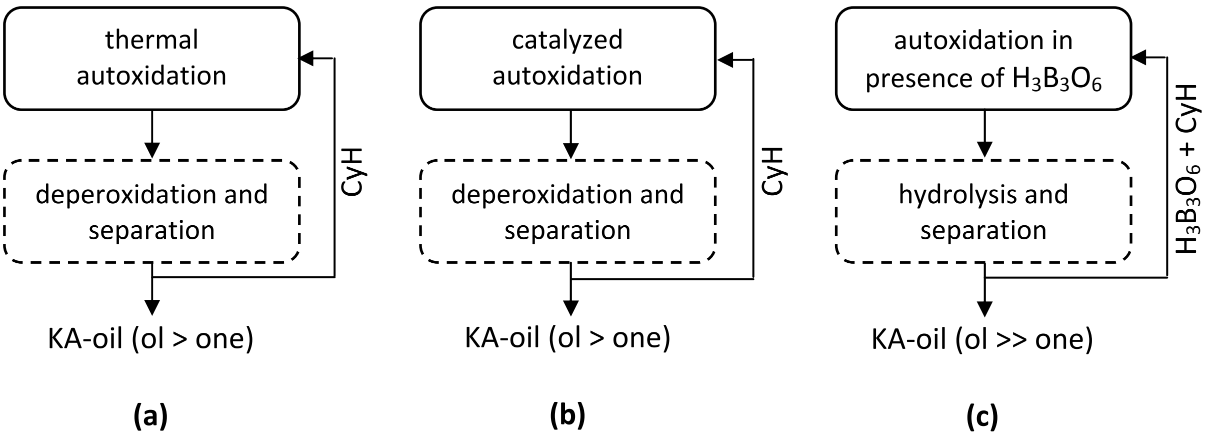

Scheme 1-5. Three different industrial cyclohexane autoxidation strategies.

In the third approach (Scheme 1-5c), developed in the 1950s by Scientific Design, anhydrous *meta*-boric acid ($H_3B_3O_6$) is added as a slurry to the first oxidation reactor. CyOOH is trapped *in situ* as the cyclohexyl perborate ester, $B(OOC_6H_{11})_3$. It is further hypothesized that this perborate ester reacts with cyclohexane to yield the borate ester, $B(OC_6H_{11})_3$, and additional cyclohexanol. The ester is subsequently hydrolyzed to yield cyclohexanol; the boric acid (H_3BO_3) is dehydrated to *meta*-boric acid and recycled (Scheme 1-5c). The esterification of the hydroperoxide and the alcohol protects them from over-oxidation, and allows the reaction to proceed to higher conversions (10-15%), without loss of a good selectivity (up to ≈90%, ol:one ≈10). Nevertheless, this process suffers from a higher investment and operating cost to recover and recycle the boric acid. At the moment, no heterogeneous catalyst process is used for the synthesis of KA-oil.

1.3 Scope of this Thesis

In this thesis we aim at a better understanding of the mechanism of radical-mediated chain oxidations. In order to be able to work under appropriate conditions, a reliable experimental set-up has to be designed. Chapter 2 presents the reactors and the conditions used, emphasizing on the best reactor passivation methods to avoid contamination from the reactor wall which would lead to speeding up the reaction. In chapter 3 we analyze the effect of added molecules to the thermal autoxidation of cyclohexane and the resulting reaction acceleration. We investigate the mechanism for the deperoxidation of *tert*-butyl hydroperoxide with cobalt(II) acetylacetonate as a homogeneous catalyst with the help of *in situ* UV/Vis spectroscopy in chapter 4. Chapter 5 shows the use of a Co/SiO_2 heterogeneous catalyst, which was synthesized by flame spray pyrolysis, for the aerobic oxidation of cyclohexane under high pressure conditions at 130 °C. Using different characterization methods and several tests under reaction conditions we could propose the actual active sites and confirm the stability and recyclability of the catalyst. The dissertation ends with an outlook for further research.

2

SET-UP AND PASSIVATION PROBLEM

In this chapter, the experimental set-up used to study aerobic oxidations is presented, together with appropriate safety measures. Different construction materials have been tested for their inertness towards deperoxidation; Polyether Ether Ketone (PEEK) has shown to have the lowest activity and was thus chosen as the most adequate material for the autoclave inserts.

2.1 Experimental Set-Up

2.1.1 Sensitivity to Explosion

Explosive gas mixtures are formed when hydrocarbon vapors and oxygen meet within certain limits. These mixtures may ignite if only a small energy amount (*e.g.*, electrical sparks, heat) is supplied. The lower and upper explosion limit are defined as the minimal and maximal combustible gas concentration at which an explosion can be set off.[1]

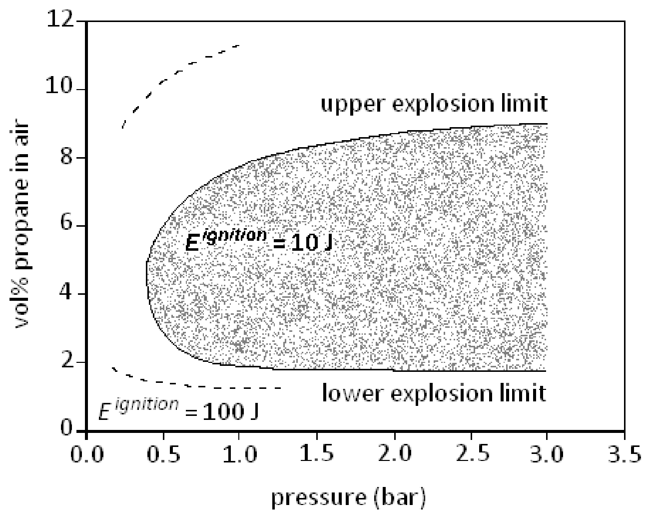

Figure 2-1. Explosion limits of propane in air as a function of the total gas pressure prior to ignition and the ignition energy *E* (10 J: solid line; 100 J: dashed line) as determined in a 7 L vessel.[16]

Figure 2-1 shows the explosion limits of propane in air as a function of the pressure of the gas composition and the ignition energy. The upper explosion limit is extended significantly by increasing either pressure or ignition energy. In contrast, the lower explosion limit is lowered only to a small extent. Most hydrocarbon-oxygen mixtures ignite without an external ignition source above a certain temperature, the so-called autoignition temperature, due to autoxidation. This ignition temperature decreases with increasing molecule chain length.[17]

A known method to lower the oxygen concentration in enclosed spaces (*e.g.*, reactors, tanks) is by dilution with inert gases, such as N_2 or CO_2. The ternary diagram in Figure 2-2 shows for instance that in principle it is possible to operate under safe conditions with air as oxidant. The grey area in Figures 2-1 and 2-2 represents the explosion range.

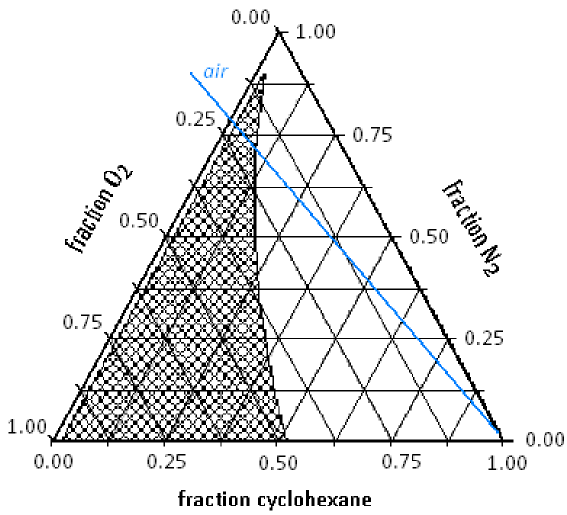

Figure 2-2. Ternary explosion diagram for cyclohexane/oxygen/nitrogen mixtures.

2.1.2 High Pressure Autoclaves and Safety

As mentioned above, hydrocarbons in contact with oxygen may lead to explosions. During autoxidation experiments potentially dangerous gas mixtures are formed, especially when operating under high pressure and high temperature conditions. Particularly during the start-up and shut-down phases, or also in case of faults, critical states may quickly arise.

The high pressure experiments were performed in 100 mL 316 stainless steel Parr® high pressure autoclaves, equipped with pressure sensor and thermocouple (Figure 2-3a and 2-4b). To avoid heterogeneous contributions from the reactor wall, an inert Polyether Ether Ketone (PEEK) insert, including a PEEK top lid, stirrer (Figure 2-3b; stirring at 200 rpm), sampling tube and cover for the thermocouple was used (see section 2.2). In this way, reproducible induction periods and conversions could be achieved (Figure 2-5).

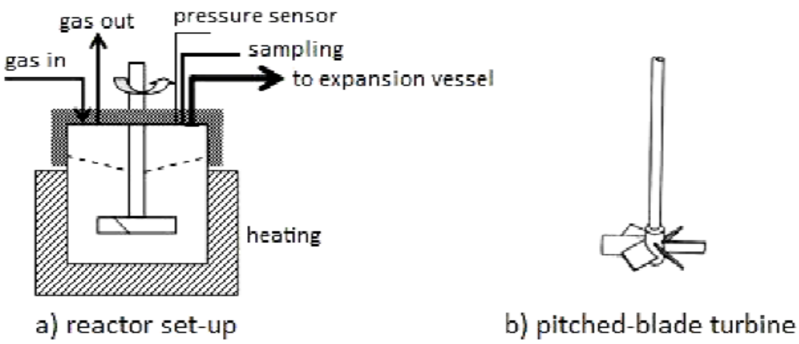

Figure 2-3. Reactor set-up (a) and stirrer type (b).

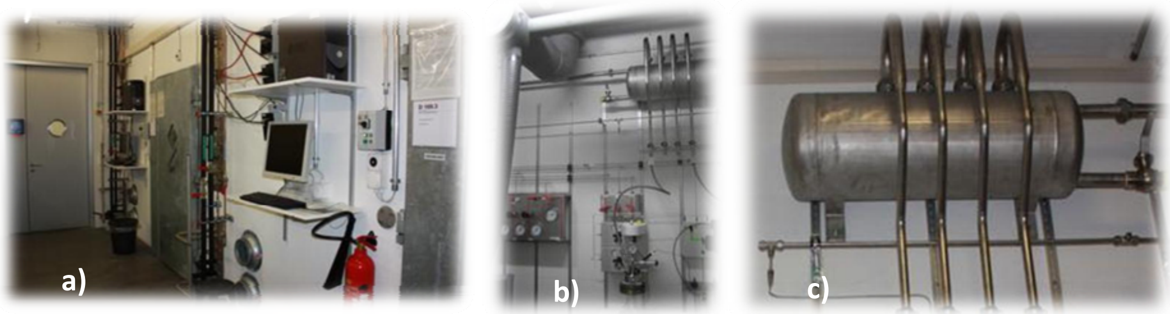

Figure 2-4. Safety measures for high pressure experiments: a) bunker cells, b) reaction set-up: 316 stainless steel Parr® high pressure autoclave, c) 20 L expansion vessel.

The reaction solution was either heated under 12 bar of N_2 to the desired reaction temperature before 6 bar of O_2 was added to start the reaction (in order to bypass explosion concentrations, Figure 2-2) or filled at room temperature with oxygen and then heated to the reaction temperature (for more details see section 3.4 and 5.2.3, respectively). Oxygen consumption was monitored by the pressure decrease.

In order to run experiments in a safe way and to protect personnel, the reactor was placed in a bunker cell and connected to a steel expansion vessel of 20 L (Figure 2-4a and 2-4c, respectively) *via* a burst plate, designed to open at 207 bar.

2.2 Reactor Passivation

It is important to realize that the reactor wall can have a significant effect on the observed activity and selectivity during lab-scale studies of oxidation reactions, due to the catalytic decomposition of the hydroperoxides, either by the reactor wall itself, or by leached metal ion species. This effect, accelerating the autoxidation rate and reducing the hydroperoxide selectivity, makes it difficult to record the correct background activity and selectivity of autoxidations. Not only for autoxidations, but actually for every peroxide-based oxidation reaction, such as epoxidations with H_2O_2, this catalytic wall effect can cause serious problems. Indeed, a Fenton-type decomposition of the peroxide on the reactor wall will not only reduce the peroxide efficiency and the overall selectivity (*viz.* the initiation of side-reactions upon the formation of undesired radicals), it can also cause a safety issue, when not anticipated, as such decomposition reactions form O_2 which can build explosive gas mixtures in the reactor. Moreover, a catalytic contribution of the reactor wall will also cause scale-up problems as the reactor surface-to-volume-ratio is inversely proportional to the reactor radius. Large scale industrial reactors are therefore much less subjective to such wall effects than small lab reactors. The design and correct operation of a reliable and robust laboratory set-up is therefore of great importance (Figure 2-5).

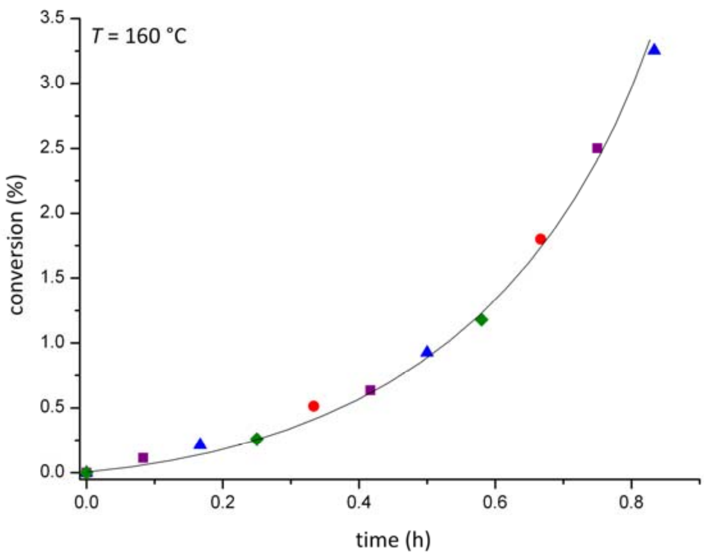

Figure 2-5. Reproducible cyclohexane autoxidation reactions at *T* = 160 °C in presence of 50 ppb homogeneous Co(II) 2-ethylhexanoate. The different colors represent different experiments in different reactors equipped with PEEK insert.

Although not generally acknowledged, peroxide solutions are intrinsically very stable, even at elevated temperatures. For example, in our hands, a 3 M aqueous H_2O_2 solution remains stable for more than 36 h at 80 °C in a carefully cleaned glass reactor. However, several materials used to construct reactors or reactor inserts cause peroxide decomposition. In order to get a more quantitative feeling for this decomposition activity, small cylindrical samples of various materials (surface area = 300 mm^2, volume = 550 mm^3) were placed in a 5 mL solution of a 3 M H_2O_2 solution in parallel glass reactors. These materials were: (i) Polyether Ether Ketone (PEEK), (ii) Teflon®, (iii) pre-passivated aluminium, (iv) stainless steel SS316, and (v) titanium. Visual inspection of the solutions shows the following reactivity towards H_2O_2 decomposition: PEEK << Teflon® < SS316 < Al < Ti. A permanganometric titration versus a sodium oxalate standard confirmed those results: the H_2O_2 decomposition after 8 h equals: <5% for PEEK, 25% for Teflon®, 30% for SS316, 40% for Al, 70% for Ti. The reason why an inert polymer such as Teflon® seems to decompose H_2O_2

is at the moment not fully clear. The hypothesis that unreacted monomer species (still containing reactive C=C bonds) would be responsible for this behavior seems to be in disagreement with the steady activity over several hours. This observation points more in the direction of H-bond activated dissociation of the H_2O_2 as previously suggested for µm Teflon® particles.[18] Also remarkable is the significant activity of the aluminium sample. Prior to its testing, the Al sample was subsequently contacted with H_2O_2/HNO_3 solutions of increasing concentration to remove traces of iron, remaining from the manufacturing process (machining) and to form a passivated Al_2O_3 layer. After several steps, the Al insert obtains indeed a non-glossy white color, indicating the formation of a passivated Al_2O_3 layer. The thickness of this layer was further extended by treating the material for 48 h in 50 wt% H_2O_2 at room temperature. The stainless steel sample was significantly more active than PEEK and Teflon®. This is important as most of the commercial high pressure reactors are constructed out of stainless steel. Interesting to note is that the activity decreases upon subsequent H_2O_2 treatments. This observation points to a self-passivation mechanism which probably involves leaching of weakly surface-bonded metal (ions), leaving behind a clean surface. The Ti sample was found to be by far the most active H_2O_2 decomposition catalyst. In solution one observes a colloidal dispersion, probably TiO_2 particles. These screening results show that even materials which one would expect to be inert are active in the (undesired) decomposition of peroxides. This implies that whenever performing peroxide-based oxidations one should carefully investigate the contribution of the reactor, especially when working in a small scale.

The autoxidation of cyclohexane is very sensitive to this sort of wall effect. Earlier, it was reported that stainless steel reactors can be passivated by contacting the metal with a saturated solution of sodium pyrophosphate.[7] However, it is important to emphasize that the reactor only becomes completely passivated after a very long time (*i.e.*, many subsequent runs of passivation and oxidation reactions). Even ppb amounts of Fenton-active ions, like iron or chromium, are able to modify the activity and selectivity during the autoxidation of cyclohexane. Especially the cyclohexanol over cyclohexanone ratio (ol/one) is very sensitive to metal catalyzed deperoxidations. An important problem is that neither the background activity of the reactor wall, nor the obtained selectivity is reproducible before the reactor is completely passivated. Similar effects were observed in reactors constructed from Hastelloy B and C.

In order to reduce the reactivity of the reactor wall, and/or to prevent leaching of metal ions, we evaluated the possibility of coating the steel with Teflon®. Three different layers of coating were subsequently applied: (i) a ground layer providing a rough sticky basic layer, (ii) an intermediate connecting layer, mainly consisting of Teflon®-Perfluoro-Alkoxy (PFA), followed by (iii) a last layer of Teflon® and cured at 410 °C for 6 min. Such a coating is routinely applied in cooking pans, but also in chemical storage tanks to make them inert towards aggressive chemicals. This approach resulted in a significant reduction of the reactivity and a remarkable improvement in the ol/one ratio. Unfortunately, the inert Teflon® layer was found to come off the wall after a few runs.

Because of the promising results with the Teflon® coating, we decided to explore the possibility of using a Teflon® insert (wall thickness 2.5 mm). Although this insert acts as an insulating barrier, resulting in an increased heating time, the cyclohexane autoxidation results were reasonable. Despite the good CyOOH selectivity, the ol/one ratio was still significantly lower than expected and not reproducible. A similar effect was observed earlier with micrometer Teflon® particles and attributed to a catalyzed conversion of the cyclohexyl hydroperoxide to cyclohexanone.[18] Of all materials tested in the decomposition of H_2O_2, the thermoplastic PEEK (Polyether Ether Ketone) showed the least activity (*vide supra*). This material is often used as an inert material with excellent mechanical strength and a lower porosity than for instance Teflon®. Cyclohexane autoxidation experiments were indeed very reproducible in PEEK inserts (Figure 2-5), resulting in a high CyOOH selectivity (around 80% at 2% conversion) and an ol/one ratio ≥1.5 (Figure 2-6).

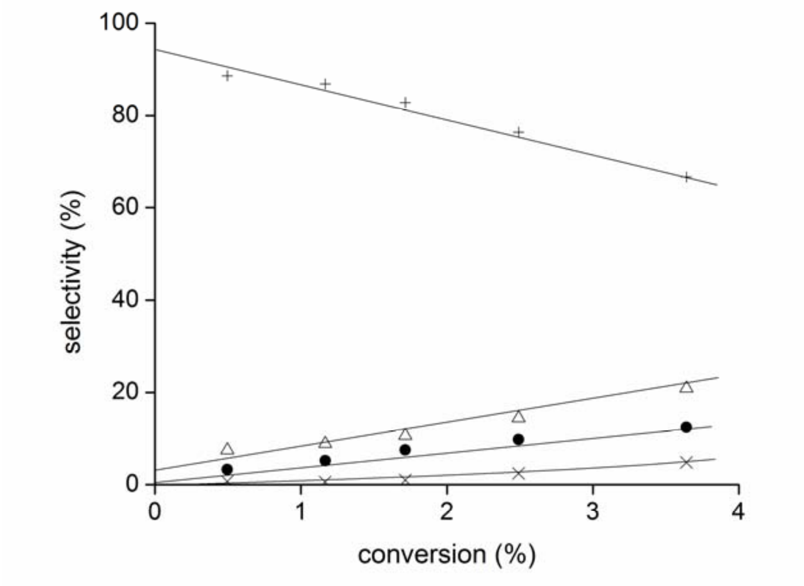

Figure 2-6. Product distribution obtained during a pure cyclohexane autoxidation experiment at 145 °C: CyOOH (*plus*), CyOH (*open triangle*), Q=O (*filled circle*) and by-products (*cross*, sum of 6-hydroxyhexanoic acid, 6-hydroperoxyhexanoic acid, adipic acid, glutaric acid and ε-caprolactone).

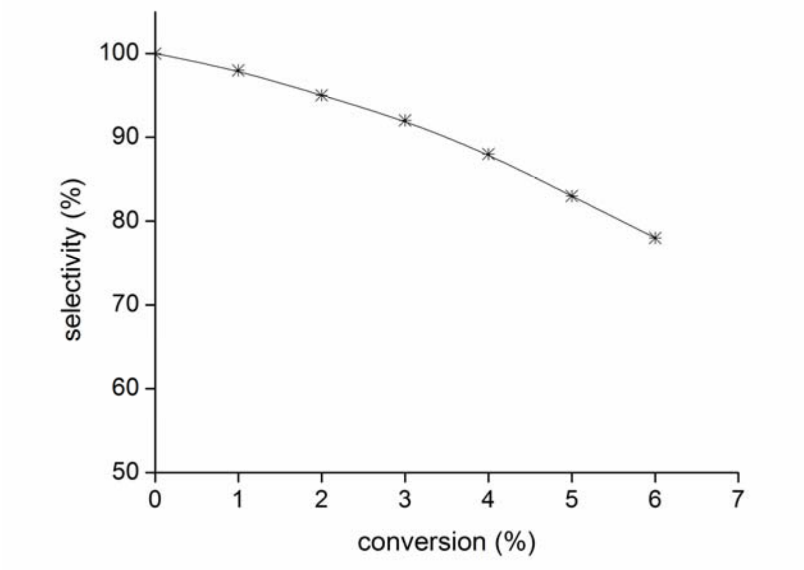

Figure 2-7. Evolution of the overall selectivity versus the conversion for a thoroughly analyzed cyclohexane autoxidation system.

It has to be emphasized that the by-products plotted in Figure 2-6 only refer to the sum of the most important by-products: 6-hydroxyhexanoic acid, 6-hydroperoxyhexanoic acid, adipic acid, glutaric acid and ε-caprolactone (Scheme 2-1). However, several other (low boiling point) by-products are additionally formed (*e.g.*, valeric acid, methanol, 1-butanol, 1-pentanol, CO, CO_2), especially at higher concentrations. Figure 2-7 shows how the selectivity depends on the conversion if both the liquid and the gas phase are thoroughly analyzed.

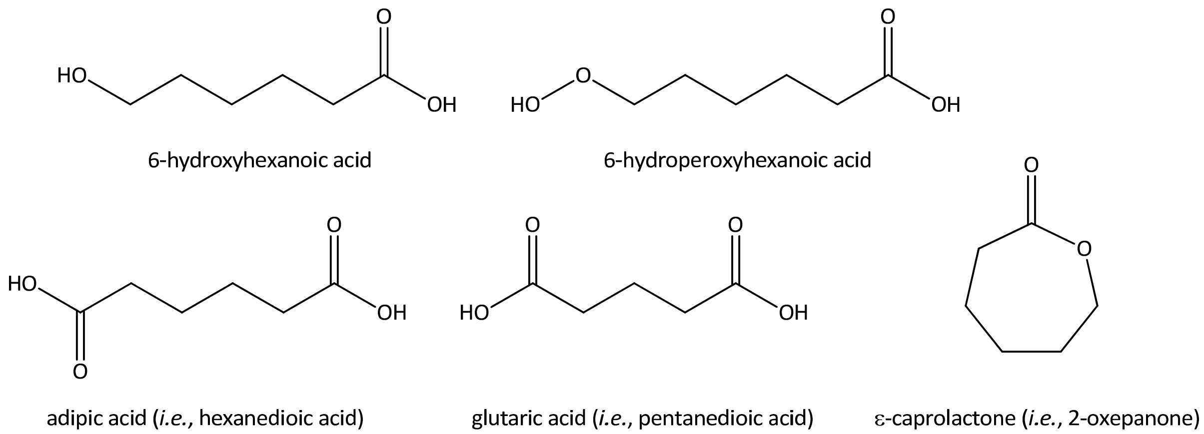

Scheme 2-1. Structures of most important by-products of cyclohexane autoxidation.

3

Influence of Additives

The homolytic cleavage of peroxide bonds, leading to the formation of free radicals, plays an important role in the (spontaneous) oxidation of a wide variety of hydrocarbons in the presence of oxygen. Such aerobic oxidations can be desired (*e.g.*, for industrially applied autoxidations) or undesired (*e.g.*, food deterioration). In this chapter we provide experimental and computational evidence for a molecule-induced homolytic dissociation mechanism between alkyl peroxide and compounds featuring weakly bonded H-atoms such as (di)unsaturated hydrocarbons.

3.1 Introduction

Free radical oxidations occur very often as undesired side-reactions, food deterioration being a typical example.[1] However, controlled autoxidations are also used on an industrial scale to produce valuable chemicals such as cyclohexanol/cyclohexanone, terephthalic acid and cumyl hydroperoxide, to mention just a few. It is well known that the rate of such reactions is greatly enhanced by minute amounts of transition metal ions, catalyzing the formation of radicals upon homolytic bond cleavage of the intermediate peroxide.[1, 19, 20] Nevertheless, even in the absence of redox-active metal species, a thermal oxidation reaction can take place. Although it was often assumed that radicals are generated upon O-O scission in the intermediate peroxides (reaction (3-1)), it was recently suggested that unimolecular cleavage is too slow and inefficient to play an important role. Alternatively, a bimolecular initiation reaction was proposed in which the OH-radical breaking away from the peroxide abstracts an H-atom from an assisting molecule (XH), leading to the formation of water (reaction (3-2); rate constant $k_{\text{init}}^{\text{XH}}$).[13] It is emphasized that the water product acts as a "spin-insulator" between the two radical products, hindering the immediate recombination to ROX. Vinyl or (bis)allyl stabilization of $X^\bullet$, as for instance encountered in unsaturated fatty acids, can significantly weaken the X-H bond, making reaction (3-2) energetically more favorable.

$$ROOH \rightarrow RO^\bullet + {}^\bullet OH \qquad (3\text{-}1)$$

$$ROOH + X\text{-}H \rightarrow RO^\bullet + H_2O + X^\bullet \qquad (3\text{-}2)$$

The $RO^\bullet$ and $X^\bullet$ radicals will subsequently react with the substrate or O_2, respectively, forming peroxyl radicals (reaction (3-3)). Those $ROO^\bullet$ radicals can propagate the radical chain (reaction (3-4)), or react among each other, partially leading to radical termination (reaction (3-5); Q=O denotes ketone).

$$R^\bullet + O_2 \rightarrow ROO^\bullet \qquad (3\text{-}3)$$

$$ROO^{\bullet} + RH \rightarrow ROOH + R^{\bullet} \quad (3\text{-}4)$$

$$ROO^{\bullet} + ROO^{\bullet} \rightarrow ROH + Q{=}O + O_2 \quad (3\text{-}5)$$

At higher conversion, the peroxyl radicals will also react with the primary hydroperoxide product, leading to substantial amounts of alcohol and ketone *via* a solvent cage assisted mechanism (see section 1.2.1). In case of cyclohexane (CyH) autoxidation, the ketone thus produced is very efficient in generating radicals *via* reaction (3-2; abstraction of the αH-atom), hence leading to an autocatalytic acceleration of the rate.[13]

The characteristic lifetime of the peroxyl radicals, $\tau(ROO^{\bullet}) = (2\ k_{term}[ROO^{\bullet}])^{-1} \approx$ 1-10 s, is significantly shorter than the timescale over which $[ROO^{\bullet}]$ changes significantly (≈ 1-30 minutes). Therefore, a steady state in peroxyl radical concentration will be approximated (equation (3-6)), arising from equating the rates of initiation (equation (3-7)) and termination (equation (3-8)).

$$[ROO^{\bullet}]_{QSS} = \sqrt{\frac{k_{init}^{XH}[XH][ROOH] + k_{init}^{CyH}[CyH][ROOH]}{k_{term}}} \quad (3\text{-}6)$$

$$R_{init} = 2\ k_{init}^{XH}[XH][ROOH] + 2\ k_{init}^{CyH}[CyH][ROOH] \quad (3\text{-}7)$$

$$R_{term} = 2\ k_{term}[ROO^{\bullet}]^2 \quad (3\text{-}8)$$

The purpose of this chapter is to provide experimental and computational evidence for the molecule-induced initiation mechanism (reaction (3-2)), in case of X-H being mono- and diunsaturated compounds. Interestingly, analogous molecule-induced homolysis has been proposed earlier by Punta *et al.* for the formation of phtalimide-*N*-oxyl radicals upon reaction of *N*-hydroxyphtalimide with peroxy acids and dioxirane (Scheme 3-1).[21-24] Nevertheless, until now unambiguous (experimental) evidence for such a mechanism is missing.

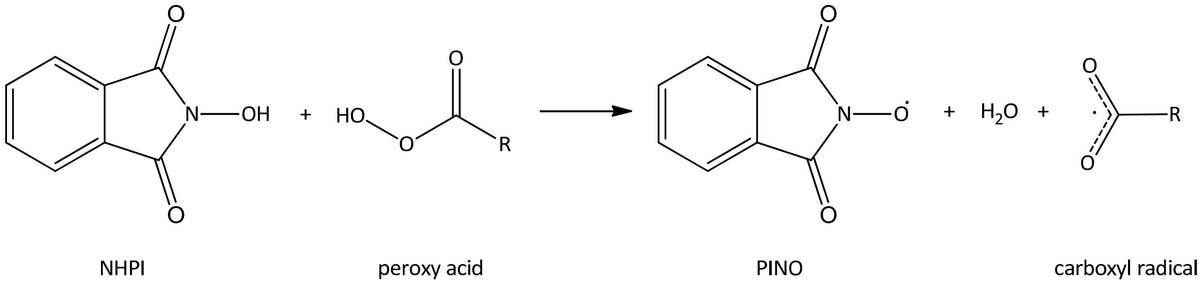

Scheme 3-1. Formation of phtalimide-*N*-oxyl radicals (PINO) upon reaction of *N*-hydroxyphtalimide (NHPI) with peroxy acids.

3.2 Results and Discussion

At low conversions (*i.e.*, below 2%), the product formation rate during an autoxidation ($\mathrm{d}\Sigma_i[P_i]/\mathrm{d}t$) is given by equation (3-9). Indeed, at such low conversions, consecutive over-oxidation of products can be neglected. After substitution of the $[\mathrm{ROO^\bullet}]_{\mathrm{QSS}}$ (equation (3-6)), equation (3-9) can be analytically integrated to equation (3-10) where α^2 is defined as the peroxide content (equation (3-11)).

$$\frac{\mathrm{d}}{\mathrm{d}t}\sum_i[P_i] = [\mathrm{ROO^\bullet}](k_{\mathrm{prop}}^{\mathrm{XH}}[\mathrm{XH}] + k_{\mathrm{prop}}^{\mathrm{CyH}}[\mathrm{CyH}]) \tag{3-9}$$

$$\sum_i[P_i] = \frac{\alpha^2}{4}\frac{k_{\mathrm{init}}^{\mathrm{XH}}[\mathrm{XH}]+k_{\mathrm{init}}^{\mathrm{CyH}}[\mathrm{CyH}]}{k_{\mathrm{term}}}(k_{\mathrm{prop}}^{\mathrm{XH}}[\mathrm{XH}] + k_{\mathrm{prop}}^{\mathrm{CyH}}[\mathrm{CyH}])^2 t^2 \tag{3-10}$$

$$\alpha^2 \equiv \frac{[\mathrm{ROOH}]}{\sum_i[P_i]} \tag{3-11}$$

Obviously, the product formation rate is proportional to the oxygen consumption rate in the system according to equation (3-12); H refers to the temperature dependent Henry coefficient ($H(T)$ = 1104 K/T).[25]

$$\sum_i[P_i]\,(t) \approx -\frac{\mathrm{d}}{\mathrm{d}t}[\mathrm{O_2}]_{\mathrm{liquid}} = \frac{1}{\mathrm{R}T}\frac{\mathrm{d}p(\mathrm{O_2})}{\mathrm{d}t}(1 + H(T)) \tag{3-12}$$

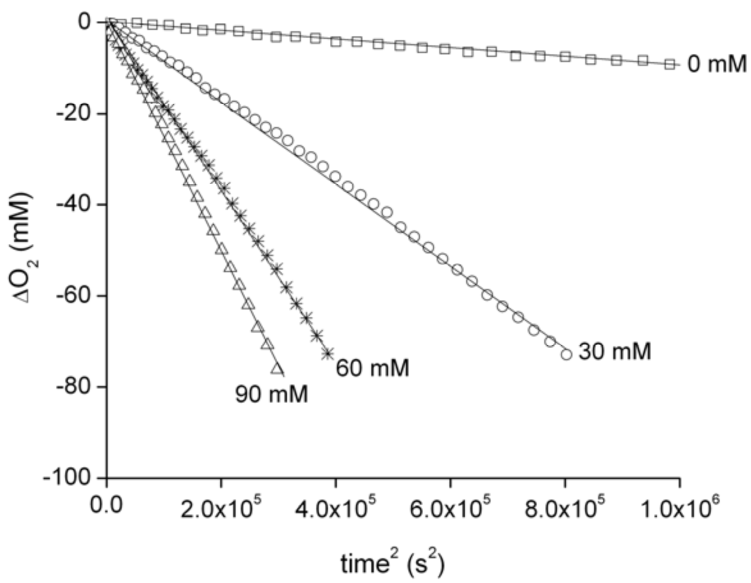

Figure 3-1. Evolution of the measured oxygen consumption in the liquid phase versus time^2 for various amounts of linoleate additive at 155 °C.

Combining equations (3-10) and (3-12) reveals a second order time behavior of the oxygen consumption rate, the latter being experimentally accessible through pressure monitoring (equation (3-12)). Figure 3-1 shows the experimental validation of these expressions, for the addition of various amounts of linoleate to a cyclohexane autoxidation reaction at 155 °C. The slope m of these plots is given by equation (3-13).

$$m = \frac{\alpha^2}{4} \frac{k_{\text{init}}^{\text{XH}}[\text{XH}] + k_{\text{init}}^{\text{CyH}}[\text{CyH}]}{k_{\text{term}}} \left(k_{\text{prop}}^{\text{XH}}[\text{XH}] + k_{\text{prop}}^{\text{CyH}}[\text{CyH}]\right)^2 \tag{3-13}$$

In Figure 3-2, m is plotted as a function of the additive concentration XH for the case of linoleate at various temperatures. The intercept I of that plot is given by equation (3-14).

$$I \equiv m([\text{XH}] = 0) = \frac{\alpha^2}{4} \frac{k_{\text{init}}^{\text{CyH}}[\text{CyH}]}{k_{\text{term}}} \left(k_{\text{prop}}^{\text{CyH}}[\text{CyH}]\right)^2 \tag{3-14}$$

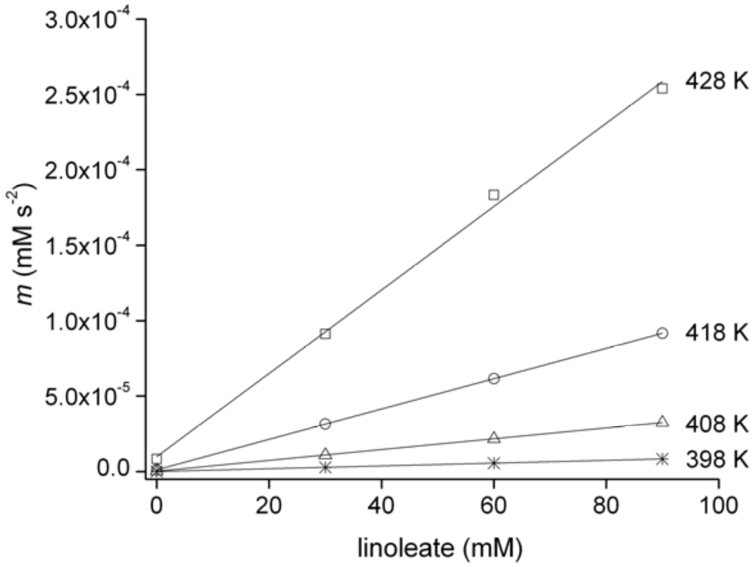

Figure 3-2. Evolution of m (equation (3-13)) versus the linoleate additive concentration at various temperatures.

The overall T-dependence of the intercept I corresponds to an Arrhenius energy of 268 ± 8 kJ mol^{-1} (see Figure 3-3). Based on the known propagation rate constant $k_{\mathrm{prop}}^{\mathrm{CyH}}(T) = 2.4 \times 10^9 \times \exp(\text{-75 kJ mol}^{-1})\ \mathrm{M}^{-1}\mathrm{s}^{-1}$ and termination rate constant $k_{\mathrm{term}} = 4 \times 10^6\ \mathrm{M}^{-1}\mathrm{s}^{-1}$, one can hence estimate the temperature dependence of the initiation rate constant $k_{\mathrm{init}}^{\mathrm{CyH}}$ (equation (3-15)).

$$k_{\mathrm{init}}^{\mathrm{CyH}}(T) = 5 \times 10^{10} \times \exp(\text{-121 kJ mol}^{-1})\ \mathrm{M}^{-1}\mathrm{s}^{-1} \qquad (3\text{-}15)$$

The value of the pre-factor (*i.e.*, 5×10^{10} M^{-1} s^{-1}) is in excellent agreement with a previous theoretical estimation, based on transition state theory calculations,[13] and reflects the loose nature of the transition state (*cfr.* the significantly extended O-O bond, *vide infra*).

S – the slope of the plots in Figure 3-2 – is given by equation (3-16).[26]

$$S \equiv \frac{\mathrm{d}m}{\mathrm{d[XH]}} \approx 3\frac{\alpha^2}{4}\frac{k_{\mathrm{init}}^{\mathrm{XH}}}{k_{\mathrm{term}}}(k_{\mathrm{prop}}^{\mathrm{XH}}[\mathrm{XH}])^2 \tag{3-16}$$

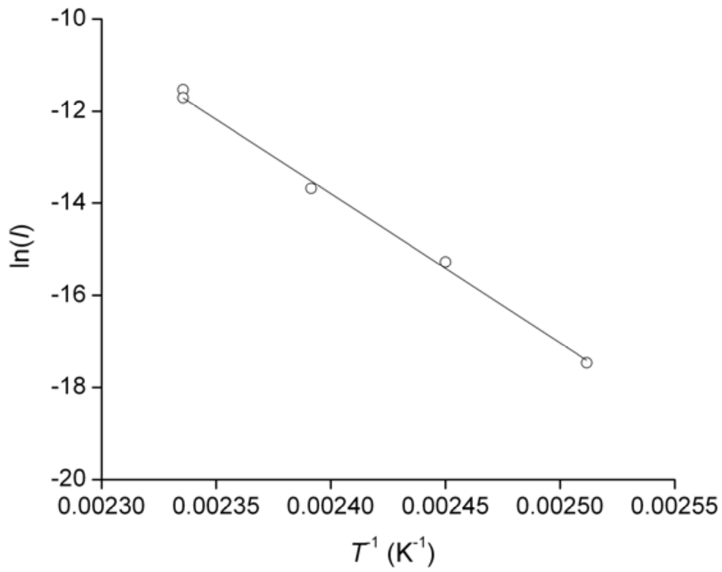

Figure 3-3. Arrhenius plot of I (equation (3-14)) for the temperature range of 125-155 °C.

Although m is in principle third order in [XH], the curvature of m versus [XH] is insignificant in the rather narrow concentration range. We emphasize that [XH] becomes temperature dependent when there is significant partitioning between gas and liquid phase, *i.e.*, when the system is close to the boiling point of XH. The actual XH concentration can be calculated according to equation (3-17) where T_0 is the normal boiling point and p_0 the normal boiling point pressure (*i.e.*, 1 atm); $\Delta_{\mathrm{vap}}H$ is the vaporization enthalpy.

$$[\mathrm{XH}]_{\mathrm{liquid}} = \frac{n(\mathrm{XH})_{\mathrm{total}}}{V_{\mathrm{liquid}}} - \exp\left(\frac{\Delta_{\mathrm{vap}}H}{\mathrm{R}}\left(\frac{1}{T_0}-\frac{1}{T}\right)\right)\frac{p_0}{\mathrm{R}T_0}\frac{V_{\mathrm{gas}}}{V_{\mathrm{liquid}}} \tag{3-17}$$

This implies that the overall T-dependence of the slope S is given by equation (3-18) where the last term only applies for compounds for which the second term in equation (3-17) cannot be neglected (*i.e.*, volatile compounds such as α-pinene, measured at T within T_0 ± 50 °C).

$$E_A(S) = E_A(k_{init}^{XH}) + 2\,E_A\left(k_{prop}^{XH}\right) - E_A(k_{term}) - \left\{2\,\Delta_{vap}H^{XH}\right\}_{XH=volatile} \quad (3\text{-}18)$$

Figure 3-4 plots the experimental T-dependence of the slope S for three different compounds; the results are summarized in Table 3-1. Combining these results with equation (3-18) leads to the estimated values for the barriers of reaction (3-2) in Table 3-1. We emphasize that the last term in equation (3-18) only affects the α-pinene case where T_0 = 155 °C and $\Delta_{vap}H$ = 46 kJ mol^{-1}.[27]

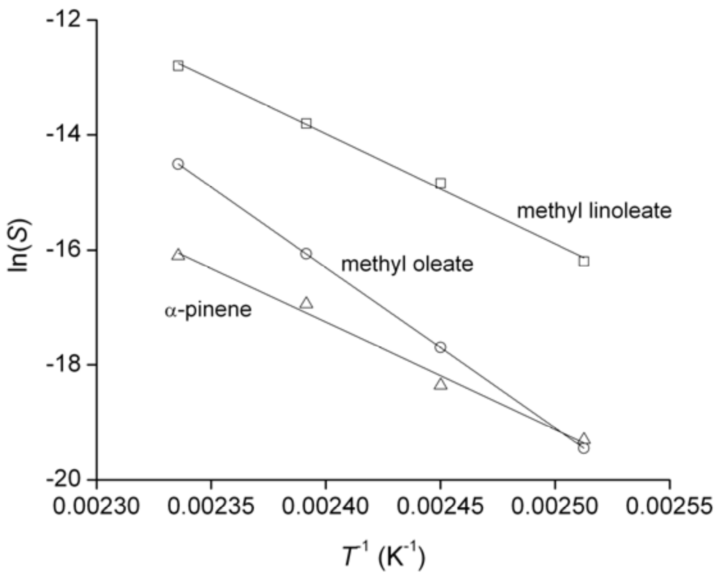

Figure 3-4. Arrhenius plot of S (equation (3-16)) for the temperature range of 125-155 °C.

Theoretical calculations at the ωB97XD-DFT level of theory,[28] taking into account long-range interactions,[29] predict barriers (Table 3-2) which are in quantitative agreement with the experimental results in Table 3-1. A linear Evans-Polanyi type correlation between the predicted barrier and heat of reaction is observed in Figure 3-5. However, compared to H-abstraction reactions by peroxyl radicals, the barrier is less sensitive to the reaction energy (*viz.* slope of 0.12 versus 0.25[1]).

Table 3-1. Experimental activation energies, determined in cyclohexane, in the T-range 125-155 °C.

compound XH	E_A (I)[a] (kJ mol^{-1})	E_A (S)[b] (kJ mol^{-1})	$E_A(k_{init}^{XH})$[c] (kJ mol^{-1})
cyclohexane	268		121 ± 13
α-pinene		151	138 ± 21
methyl oleate		234	130 ± 13
methyl linoleate		159	113 ± 13

[a] see Figure 3-3; [b] see Figure 3-4; [c] as derived from equations (3-15) and (3-18).

Table 3-2. Computed adiabatic barrier E_b and reaction energy $\Delta_r E$ for reaction (3-2) and the O-O distance in the transition state (Scheme 3-2).[a]

compound XH	computed $E_b(k_{init}^{XH})$ (kJ mol^{-1})	d(O-O) (Å)	*imaginary frequency* (i^2 cm^{-1})	Computed $\Delta_r E$[b] (kJ mol^{-1})
cyclohexane	131.4	2.10	1047	62.8
α-pinene	125.5	1.98	1230	0.8
methyl oleate[c]	125.5	1.97	1273	-7.1
methyl linoleate[c]	116.7	1.88	1556	-48.5

[a] ωB97XD/6-311++G(df,pd) level of theory; [b] for reaction (3-2); [c] (*Z*)-hex-2-ene and (*Z*,*Z*)-hepta-2,5-diene were used as convenient models for methyl oleate and linoleate, respectively.

The reason why the activation barrier is less sensitive to the C-H bond strength is due to the fact that the reaction coordinate is mainly composed of the O-O distance (see also *imaginary frequency* in Table 3-2) which is lower than for a pure H-abstraction reaction.

Indeed, whereas a good correlation between the O-O distance and the barrier can be observed in Figure 3-5, the C-H distance remains 1.23 ± 0.01 Å for all investigated cases.

Combining the predicted barrier of 125.5 kJ mol^{-1} for α-pinene (Table 3-2) with the estimated pre-factor of 5 $\times$ 10^{10} M^{-1} s^{-1} (equation (3-15)) leads to an extrapolated $k_{\text{init}}^{\text{α-pinene}}$(363 K) value of 5 $\times$ 10^{-8} M^{-1} s^{-1}. This number is in fair agreement with the value stemming from a numerical modeling simulation of the overall α-pinene autoxidation kinetics at 363 K (*i.e.*, 4 $\times$ 10^{-7} M^{-1} s^{-1}).

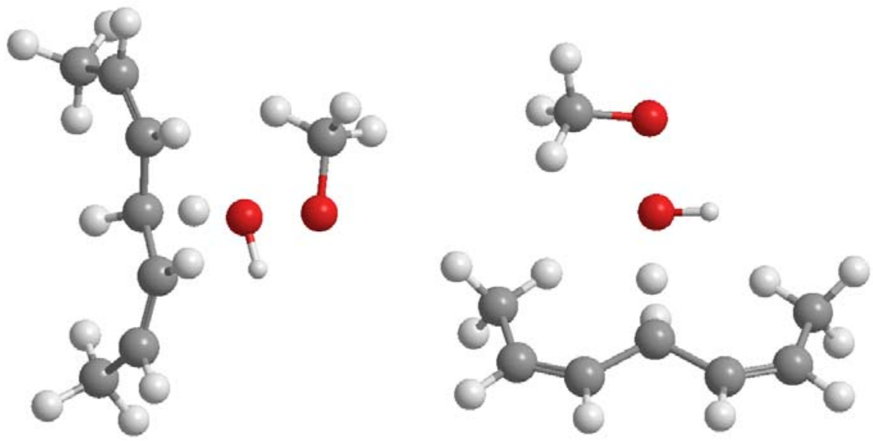

Scheme 3-2. Transition state resulting during reaction (3-2); the hydroxyl radical breaking away from the peroxide abstracts an H-atom from an assisting molecule, leading to water and two active radicals. (*Z*,*Z*)-hepta-2,5-diene was used as convenient model for methyl linoleate.

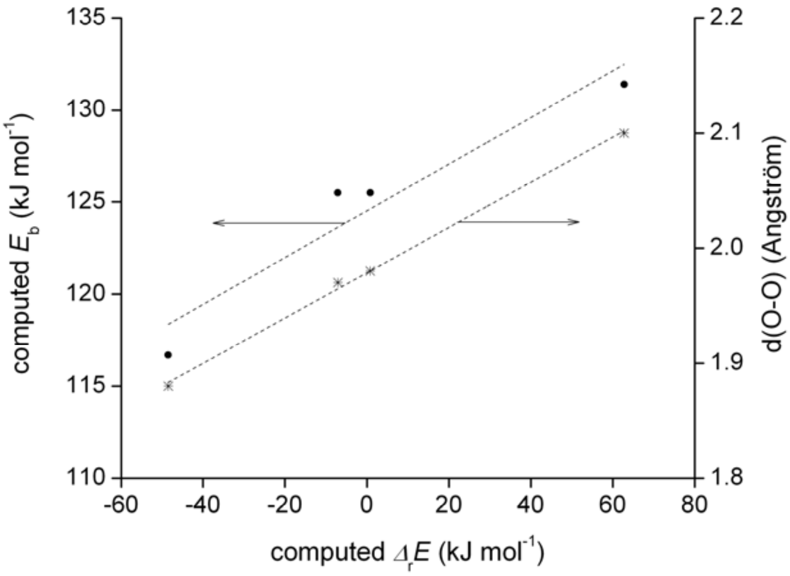

Figure 3-5. Evans-Polanyi type correlation between the predicted barrier and heat of reaction (3-2) as well as the O-O distance in the transition state (see Table 3-2).

3.3 Conclusion

Compounds featuring weakly bonded H-atoms in allylic position are efficient in generating radicals upon reaction with hydroperoxide molecules. Indeed, the OH-radical breaking away from the hydroperoxide molecule can abstract an H-atom, yielding water plus an alkoxyl and alkyl radical. The loose transition state, due to an almost broken O-O bond, results in a large pre-exponential rate factor. The main compound of the reaction coordinate is the O-O bond distance, resulting in only a moderate dependence of the adiabatic barrier on the C-H bond strength, compared to classical H-abstractions by peroxyl radicals where the C-H bond cleavage plays a pivotal role. The results of this study indicate that substrates which are susceptible to autoxidation, such as unsaturated fatty esters like oleate or linoleate, are not only reacting very rapidly with radicals, they are also faster in generating radicals *via* the described mechanism.

3.4 Experimental Section

Experiments were performed in a 100 mL 316 stainless steel Parr® high pressure reactor, equipped with an inert Polyether Ether Ketone (PEEK) insert, including a PEEK top lid and stirrer (see section 2.1.2). The cyclohexane solution containing a known amount (0-90 mM) of additive (α-pinene, methyl oleate or methyl linoleate) was heated under 12 bar of N_2 to the desired reaction temperature (398-428 K) before 6 bar of O_2 was added to start the reaction. Oxygen consumption was monitored by the pressure decrease. Quantum chemical calculations were performed with the Gaussian09 software (version A.02)[30] at the ωB97XD/6-311++G(df,pd) level of theory.[28, 29] The reported relative energies were corrected for zero point energy (ZPE) differences. (*Z*)-hex-2-ene and (*Z*,*Z*)-hepta-2,5-diene were used as convenient models for methyl oleate and linoleate, respectively.

4

HOMOGENEOUS CATALYSIS

The Co^{II}/Co^{III}-induced decomposition of hydroperoxides is an important reaction in many industrial processes and is referred to as deperoxidation. In the first step of the Fenton-type reaction cycle, alkoxyl radicals and Co^{III}-OH species are generated upon the reaction of the Co^{II} ion with ROOH. The catalytic cycle is closed upon the regeneration of the Co^{II} ion through the reaction of the Co^{III}-OH species with a second ROOH molecule, thus producing one equivalent of the peroxyl radicals. Herein, the deperoxidation of *tert*-butyl hydroperoxide by dissolved cobalt(II) acetylacetonate is studied by using UV/Vis spectroscopy *in situ* with a noninteracting solvent, namely, cyclohexane. Kinetic information extracted from experiments, together with quantum-chemical calculations, led to new mechanistic hypotheses. Even under anaerobic conditions, the Fenton-type cycle initiates a radical chain destruction of ROOH propagated by both alkoxyl and peroxyl radicals. This chain mechanism rationalizes the high deperoxidation rates, which are directly proportional to the cobalt concentration.

4.1 Introduction

Cobalt complexes that are soluble in the reaction mixture are used for converting the (remaining) alkyl hydroperoxide (ROOH) intermediate of the hydrocarbon autoxidation reaction into additional alcohol (ROH) and ketone (Q=O) species (*i.e.*, homogeneous catalysis).[1] During this peroxide activation reaction, several reactive oxidizing species (*i.e.*, oxygen-centered radicals) are generated, thus explaining why ROOH can also be used as an oxidant in metal-catalyzed (ep)oxidations.[31] The cobalt-induced cleavage of ROOH is also an important step in the (chemical) drying of alkyd paint.[32] Indeed, the spontaneous aerobic oxidation of binder molecules containing unsaturated C=C bonds (fatty acid chains) produces allylic hydroperoxides, the cobalt-induced decomposition and subsequent chemistry of which causes cross-linking between the binder molecules, thus shortening the drying time.

According to previous reports, cobalt ions react with ROOH in a Fenton-type catalytic cycle (reactions (4-1) and (4-2)), thus resulting in an overall conversion of two ROOH molecules in alkoxyl ($RO^{\bullet}$) and peroxyl ($ROO^{\bullet}$) radicals (reaction (4-3)).[33, 34]

$$Co^{II} + ROOH \rightarrow Co^{III}\text{-}OH + RO^{\bullet} \tag{4-1}$$

$$Co^{III}\text{-}OH + ROOH \rightarrow Co^{II} + H_2O + ROO^{\bullet} \tag{4-2}$$

$$2\ ROOH \rightarrow RO^{\bullet} + ROO^{\bullet} + H_2O \tag{4-3}$$

According to this two-step mechanism, the Co^{II} ion is first oxidized by ROOH to a Co^{III}-OH intermediate, which can be regenerated back to the starting Co^{II} ion upon reaction with a second ROOH molecule (see section 1.2.2). At the moment, there is disagreement over which step (*i.e.*, reaction (4-1) or (4-2)) is the rate-determining step, and hence which cobalt species (*i.e.*, Co^{II} or Co^{III}-OH) is the dominant in solution.[35, 36] Little information is available on the precise rate or temperature dependence of the reactions. There is even controversy about the active species, that is, the monomeric or μ-oxo/μ-hydroxo-bridged species.[37] The mechanism has not been unambiguously clarified. A solid mechanistic understanding of the chemistry would be useful to guide process optimization and the development of more efficient (heterogeneous) catalytic systems.[38-40]

Herein, the deperoxidation of *tert*-butyl hydroperoxide (denoted below as ROOH) by the homogeneous model catalyst cobalt(II) acetylacetonate ([Co(acac)$_2$]) is kinetically characterized in a noninteracting solvent, namely, cyclohexane. The main goal of this chapter is to quantify the kinetics and to gain insight into the fundamental chemistry of this reaction.

4.2 Results and Discussion

4.2.1 Introduction to the Experiments

tert-Butyl hydroperoxide (5.5 M in decane, dried over molecular sieves (4 Å)) was used as a model hydroperoxide because of its lack of an α-H atom, the abstraction of which could significantly complicate the chemistry. Because hydroperoxides can form double H-bonded dimers,[41] the ROOH concentration was chosen to be low enough so that the population of the dimers can be neglected in the studied temperature range. Indeed, the dimers might have a different reactivity to the monomers. In the case of *tert*-butyl hydroperoxide, the MPW1B95/6-31+G(d,p)[42] predicted zero point energy (ZPE) corrected stability of the dimer at 0 K was 33 kJ mol^{-1} with respect to the separated monomers. This finding implies that for the ROOH concentrations used in this study (*i.e.*, below 10 mM), the dimer fraction can be neglected, even at a temperature as low as 323 K. For the same reason, ROOH was diluted in a noninteracting solvent (*i.e.*, cyclohexane (CyH)).

Although the precise deperoxidation rate was unknown at the start of this study, it can be anticipated that the reaction must be fast, even at room temperature (compare with the paint drying process). Offline analysis (*e.g.*, by conventional gas chromatography) could generate less reliable kinetic data; therefore, the reaction should preferably be monitored *in situ*. Given the low catalyst and substrate concentrations, sensitive UV/Vis spectroscopy was selected to follow the reaction (see section 4.4).

4.2.2 Spectral Observations

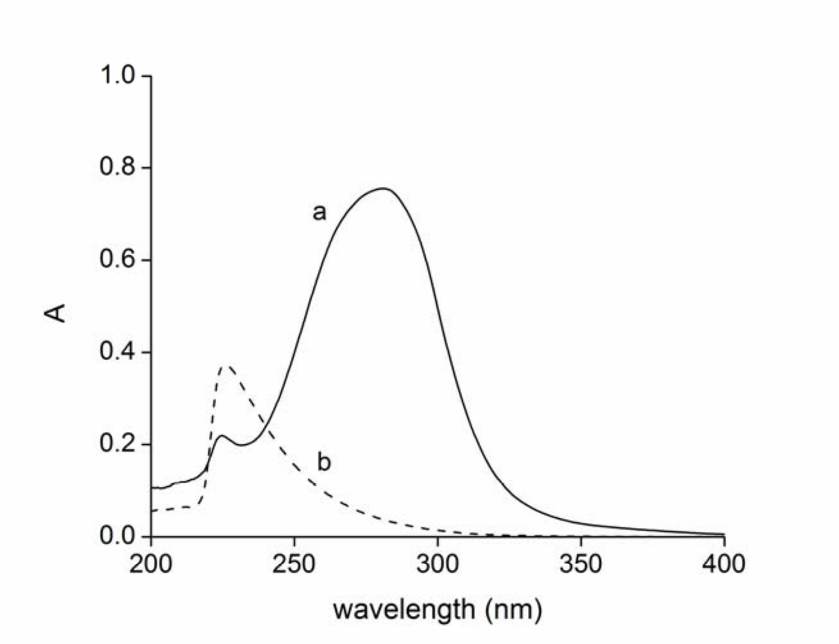

Figure 4-1. UV/Vis spectra of a) 50 µM [Co(acac)$_2$] and b) 10 mM ROOH in cyclohexane at 343 K.

The UV/Vis spectrum of [Co(acac)$_2$] in cyclohexane shows a broad absorption band between λ = 250 and 320 nm and a weak feature at λ = 225 nm (Figure 4-1). (Note that the band at λ = 225 nm was probably underestimated due to the decreased transparency of the sapphire windows below λ = 220 nm.) Although the latter signal from [Co(acac)$_2$] interferes with the absorption by ROOH in this wavelength region (Figure 4-1), the consumption of ROOH can still be monitored by the absorbance signal at λ = 225 nm, which is linear in [ROOH] (see section A.1 in Appendix A). It can indeed be expected that the concentrations of cobalt species approach a steady state for the duration of the experiment so that spectral changes at λ = 225 nm can be mainly attributed to the consumption of ROOH.

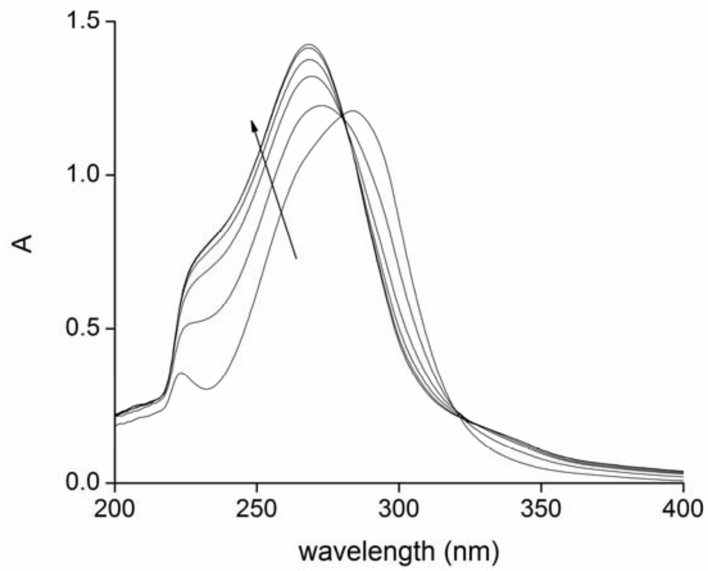

Figure 4-2. Effect of the addition of cyclohexanol (0, 20, 40, 60, 80, 100 mM) on the spectrum of 85 µM [Co(acac)$_2$] at room temperature. Note the isosbestic points at λ = 280 and 320 nm.

As the absorption cross-section of the alcohols is much lower than that of ROOH and [Co(acac)$_2$], the ROH product does not directly interfere in the spectroscopic measurements. Nevertheless, alcohols such as cyclohexanol (CyOH) seem to induce a significant blue shift when added to a solution of [Co(acac)$_2$] in cyclohexane (Figure 4-2). The appearance of two isosbestic points (λ = 280 and 320 nm) demonstrates that under the experimental conditions, alcohols can coordinate to the cobalt ions. This behavior points either to the presence of vacant coordination sites in the [Co(acac)$_2$] species or to a very rapid ligand exchange reaction taking place. Given the high purity of the solvent and the hydrophilicity of cobalt ions, the most likely other ligand is water. However, attenuated total reflection infrared (ATR-IR) measurements of the starting [Co(acac)$_2$] powder showed no evidence for the presence of water. Moreover, the solubility of H_2O is very low in CyH, thus rendering the possibility of additional water ligands (besides the acetylacetonate ligands) small. This hypothesis is supported by a similar and gradual blue shift in the [Co(acac)$_2$] spectrum in CyH upon the addition of small quantities of water (in total below 100 mM), thus also leading to an isosbestic point at λ = 277 nm. These observations suggest that the [Co(acac)$_2$] species present in CyH have unoccupied coordination sites.

The coordination of alcohol is probably one of the main reasons why alcohols tend to inhibit cobalt catalyzed autoxidation and deperoxidation reactions. Therefore, the deperoxidation of ROOH has to be studied under initial kinetic conditions, that is, at low conversions. The stability of the [Co(acac)$_2$]/methanol complex is computationally predicted to be 41.8 and 31.8 kJ mol^{-1} at the UB3LYP/LANL2DZ and UBP86/LANL2DZ levels of theory, respectively. The fact that both DFT functionals – each with its own shortcomings – agree within a few kJ mol^{-1} on the stability of the complex is an indication that this prediction is rather reliable. Moreover, the average stability of ≈38 kJ mol^{-1} is in qualitative agreement with the observed shift in Figure 4-2.

4.2.3 Time-Resolved Measurements after the Addition of ROOH

The addition of ROOH to [Co(acac)$_2$] in solution immediately induces similar spectroscopic changes as the addition of alcohol, thus indicating that ROOH also coordinates to the cobalt ions (Figure 4-3). Note that the initial strong increase of the absorption signal at around λ = 230 nm upon the addition of ROOH is caused by (i) ROOH itself and (ii) coordination of ROOH to the Co^{II} ion. Indeed, a comparison of Figures 4-1 and 4-3 shows that the absorbance of [Co(acac)$_2$]/ROOH in solution is greater (especially at around λ = 250 nm) than the algebraic sum of the absorbances of the two separate solutions. The stability of the [Co(acac)$_2$]/CH_3OOH complex is computationally predicted to be 27.2 and 26.4 kJ mol^{-1} at the UB3LYP/LANL2DZ[43] and UBP86/LANL2DZ[44] levels of theory, respectively. This finding is ≈10.5 kJ mol^{-1} weaker than for the alcohol complex. This relative difference seems to be significant, given the close agreement between the UB3LYP- and UBP86-predicted stabilities of both complexes. However, it was observed that a significantly lower amount of ROOH can induce a similar spectroscopic shift to that observed for ROH. This observation could point towards the formation of other cobalt species that induce a similar blue shift, such as Co^{III}-OH and/or Co^{III}-OOR.

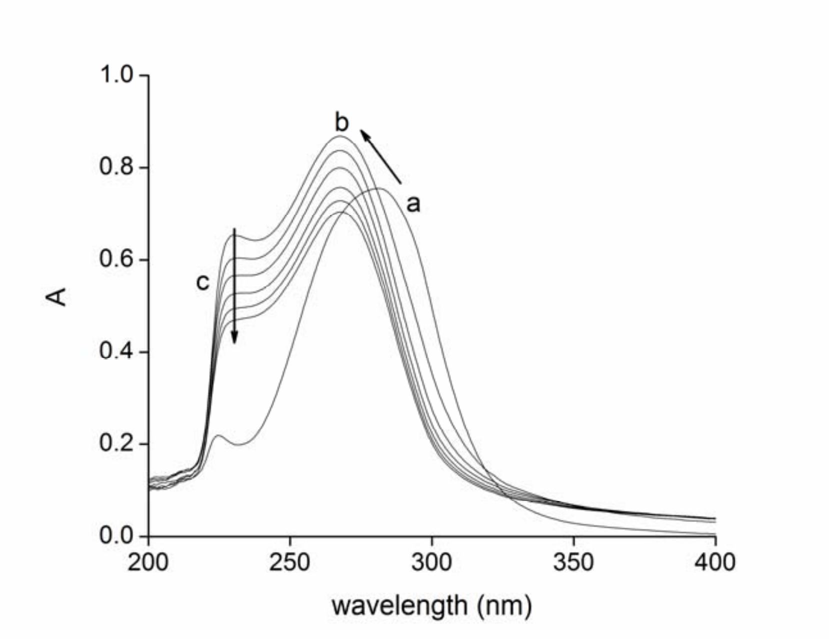

Figure 4-3. a) Spectrum of 50 µM $[Co(acac)_2]$ in CyH at 343 K. b) Instantaneous spectral shift upon the addition of 10.0 mM *tert*-butyl hydroperoxide (t = 0), in part due to the coordination of Co^{II} ions by ROOH. c) The subsequent decrease of absorbance as a function of time, which was uniform over the spectral range and due to the chemical removal of ROOH (spectra recorded every 60 s).

Immediately after the instantaneous spectral shift, the absorbance starts to decrease with time over the entire range λ = 220–350 nm due to consumption of ROOH (Figure 4-3). Although the absolute ROOH decay cannot be measured due to the anticipated spectral interference of, *e.g.*, the Co^{II}/ROOH complex, the relative concentration of ROOH can still be followed because [Co^{II}/ROOH] is expected to be proportional to [ROOH]. The kinetic plots in

Figure 4-4 unambiguously demonstrate first order kinetics for ROOH. To avoid inhibition by coordination of the alcohol product to the cobalt species (see above), the reaction was monitored only until [ROOH](t)/[ROOH](0) ≈ 0.5 (*i.e.*, initial kinetics). As an example, the pseudo first order rate constant $k' \equiv$ -dln{[ROOH](t)/[ROOH](0)}/dt at 343 K with 50 μM [Co(acac)$_2$] equals 2.0×10^{-3} s^{-1}. Note that the absence of an induction period indicates that the species initially present are immediately active in the catalytic deperoxidation. Fast and irreversible catalyst deactivation can be excluded in the studied conversion range because the pseudo first order rate constants do not change as a function of time, that is, the slope of the plot of ln{[ROOH](t)/[ROOH](0)} versus time does not show any measurable decrease.

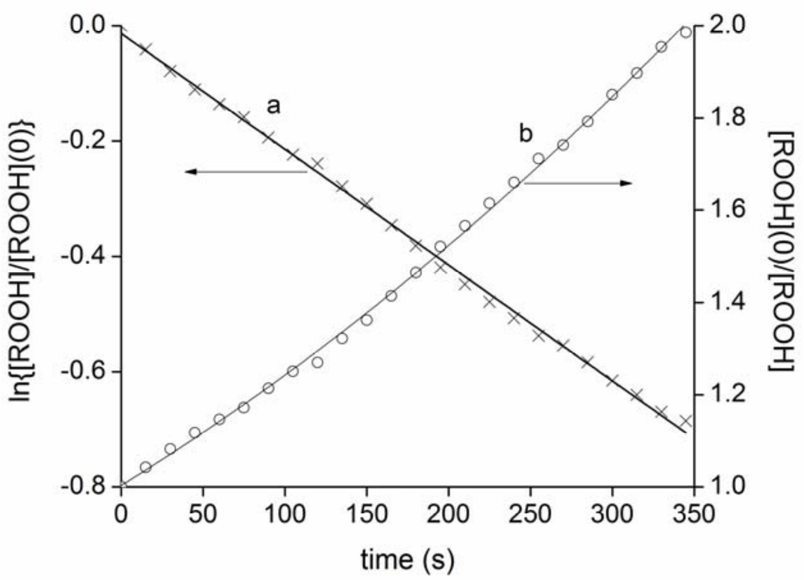

Figure 4-4. a) First order and b) second order kinetic plots of the deperoxidation of ROOH by 50 μM [Co(acac)$_2$] at 343 K; [ROOH](0)= 10.0 mM. Determination of the pseudo first order rate constant $k' \equiv$ -dln{[ROOH](t)/ [ROOH](0)}/dt = 2.0×10^{-3} s^{-1}.

4.2.4 Kinetic Quantification at 323-343 K

A number of measurements of the rate of ROOH removal was carried out at various concentrations of the $[Co(acac)_2]$ catalyst at three different temperatures (*i.e.*, 323, 333, and 343 K; Figure 4-5). This plot demonstrates the first order kinetics in the concentration of $[Co(acac)_2]$. The experiments were limited to 323-343 K because ROOH dimers could become important at lower T values, whereas the reaction becomes too fast for accurate monitoring with the applied set-up at higher T values. However, this narrow T range is compensated by the precision of the data. The apparent overall bimolecular rate coefficient $k(T)$ was obtained from the plots of $k' \equiv$ -dln[ROOH](t)/[ROOH](0)}/dt versus $[Co(acac)_2]$. An Arrhenius plot of ln{$k(T)$} versus $1/T$ is inserted in Figure 4-5; the data can be fitted with excellent precision by the Arrhenius expression $k(T) = 1.2 \times 10^{10} \times \exp(-54\ \text{kJ mol}^{-1}/RT)$ $M^{-1}\ s^{-1}$.

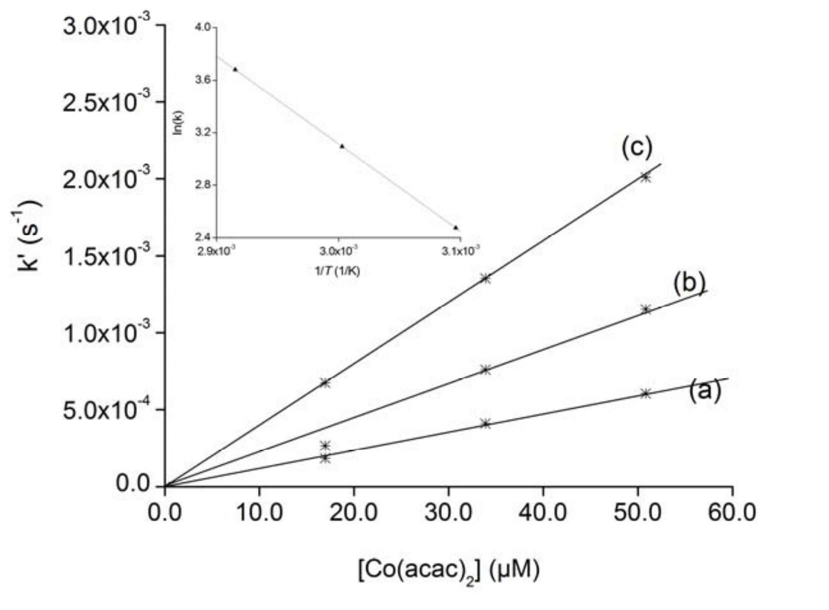

Figure 4-5. Pseudo first order rate constant for the deperoxidation of ROOH $k' \equiv$ -dln [ROOH](t)/[ROOH](0)}/dt as a function of the $[Co(acac)_2]$ catalyst concentration at different temperatures: a) 323, b) 333, and c) 343 K. The insert shows the Arrhenius plot of the apparent overall bimolecular rate coefficient $k(T)$.

We emphasize that the Arrhenius frequency factor (*i.e.*, A_{Arrh} = 1.2 × 10^{10} M^{-1} s^{-1}) is strikingly large. This outcome seems to indicate that the experimental findings are irreconcilable with the Fenton-type mechanism as the sole sink of ROOH, even allowing for the consumption of two additional ROOH molecules by the fast subsequent reactions (4-1) and (4-5; see below). One must indeed conclude that the observed deperoxidation rate is approximately one order of magnitude higher than expected for a pure Fenton-type mechanism. The most probable rationalization is a chain mechanism, initiated by the Fenton-type cycle.

4.2.5 Reaction Mechanism

Rationalization of the experimental observations starts by examination of the fate of the alkoxyl radicals produced in reaction (4-1). The $RO^{\bullet}$ radical can either react with the cyclohexane solvent (reaction (4-4)) or with the hydroperoxide (reaction (4-5)).

$$RO^{\bullet} + CyH \rightarrow ROH + Cy^{\bullet} \quad (4\text{-}4)$$

$$RO^{\bullet} + ROOH \rightarrow ROH + ROO^{\bullet} \quad (4\text{-}5)$$

The rate of reaction (4-4) was measured at 253-302 K;[45] slight extrapolation predicts k_4(333 K) to be as large as (1.5 ± 0.5) × 10^6 M^{-1} s^{-1}. However, reactions of the type $X^{\bullet}$ + ROO-H → X-H + $ROO^{\bullet}$ are also known to be surprisingly fast.[46] Calculations at the UB3LYP/6-311++G(df,pd)//UB3LYP/6-31G(d,p) level, which are known to predict quantitatively reliable barriers for H-transfer reactions,[7] demonstrate that reaction (4-5) proceeds *via* a transition state (TS) that is located 12.34 kJ mol^{-1} below the level of the reactants (a so-called submerged TS) due to the formation of strong pre- and post-reactive H-bonded complexes. The rate constant of reaction (4-5) predicted by TS theory (TST) would therefore be approximately 3 × 10^{10} M^{-1} s^{-1}, given the average pre-exponential rate constant for H-transfer reactions of 3 × 10^8 M^{-1} s^{-1}.[11] This estimation of k_5 is one order of magnitude larger than the normal diffusion controlled rate constant. Therefore, one has to estimate the precise rate at which the $RO^{\bullet}$ radical and ROOH diffuse towards each other, rather than using this TST value. Based on the long-range $ROOH\cdots{}^{\bullet}OR$ dipole-dipole interaction and by adopting as a "reactive distance" – the separation of the reactants at which the interaction energy equals $k_B T$ – the diffusion limited rate constant k_5(333 K) can be estimated to be 2×10^{10} M^{-1} s^{-1}.[47] This rate is significantly faster than diffusion controlled reactions between non-polar reactants in aqueous solutions (*i.e.*, usually ≈ 3×10^9 M^{-1} s^{-1}) but only slightly faster than, for example, the measured recombination of iodine atoms in hexane (*i.e.*, 1.3×10^{10} M^{-1} s^{-1}),[48] in which no long-range interactions are at play. The known or estimated rate constants of reactions (4-4) and (4-5) imply that under the experimental conditions (*i.e.*, [CyH] = 9.5 M and initial [ROOH] = 10^{-2} M) the majority of the $RO^{\bullet}$ radicals react rapidly (within ≈ 3 ns) with ROOH to form $ROO^{\bullet}$ radicals and ROH. This conclusion is in line with Visser and co-workers, who studied the consumption of *tert*-butyl hydroperoxide by *tert*-butoxyl radicals generated by the thermal dissociation of di-*tert*-butyl peroxyoxalate at 318 K.[49]

We will return to the fate of the 5-10% $Cy^{\bullet}$ radicals formed in reaction (4-4). Furthermore, β-scission of the *tert*-butoxyl radical can be neglected in the experimental T range.[45]

Note that when reaction (4-4) is neglected (see above), the rate controlling reaction (4-1) and the two (fast) subsequent reactions (4-2) and (4-5) can be combined into one overall catalytic initiation reaction controlled by k_1 (*i.e.*, Co^{II} + ROOH (+ 2 ROOH) $\rightarrow$ Co^{II} + ROH + H_2O + 2 $ROO^{\bullet}$), with the rate of chain initiation (*i.e.*, $R_{init} = k_1[Co^{II}][ROOH]$; as a single chain involves two $ROO^{\bullet}$ radicals; see below), but with the rate of ROOH removal due to the initiation (equation (4-6)):

$$(-d[ROOH]/dt)_{init} = 3\, k_1[Co^{II}][ROOH] \qquad (4\text{-}6)$$

For $ROO^{\bullet}$ radicals, two competing pathways are possible: the self-reactions (4-7a) and (4-7b) and the H-abstraction reaction with the solvent (reaction (4-8)).

$$ROO^{\bullet} + ROO^{\bullet} \rightarrow RO^{\bullet} + RO^{\bullet} + O_2 \qquad (4\text{-}7a)$$

$$ROO^{\bullet} + ROO^{\bullet} \rightarrow ROOR + O_2 \qquad (4\text{-}7b)$$

$$ROO^{\bullet} + CyH \rightarrow ROOH + Cy^{\bullet} \qquad (4\text{-}8)$$

The self-reaction of *tert*-butyl peroxyl radicals – as is the case with all tertiary peroxyl radicals – produces mainly $RO^{\bullet}$ radicals, whereas termination to form ROOR is only a minor channel, relative to the reactions of primary and secondary peroxyl radicals in which α-H atoms can be transferred.[3] Indeed, for tertiary peroxyl radicals, termination only occurs for a small fraction as a result of in-cage recombination of the nascent $RO^{\bullet}$ radicals prior to their diffusive separation.[46] The total rate constant for the mutual reaction of two *tert*-butyl peroxyl radicals in the gas phase is known to be $k_{7,gas}$(333 K) = 8×10^4 M^{-1} s^{-1}.[50] In a noninteracting liquid, TST predicts the bimolecular rate constants to be approximately three times larger due to smaller translation partition functions of all the involved species in the liquid phase.[51] Therefore, a reasonable estimate of k_7(333 K) is approximately 3×10^5 M^{-1} s^{-1}. This quantity is important because reaction (4-7a) becomes the rate controlling propagation step in the overall mechanism of ROOH removal because each resulting $RO^{\bullet}$ radical rapidly attacks an ROOH molecule through reaction (4-5). By attributing the observed deperoxidation rate (*i.e.*, 1.1×10^{-5} M s^{-1} at 50 µM [$Co(acac)_2$] and 333 K; see above) mostly to the chain propagation (*i.e.*, neglect the initiation as a sink for ROOH) and using the value of $k_{7a} \approx k_7$ (see above), [$ROO^{\bullet}$] can be estimated to be approximately 4×10^{-6} M. The competing $ROO^{\bullet}$ sink, namely, reaction (4-8), is characterized by the rate constant k_8(333 K) $\approx 3 \times 10^2$ M^{-1} s^{-1}.[1, 52] Given the estimated [$ROO^{\bullet}$] of approximately 4×10^{-6} M, the rate of reaction (4-8) should be close to 1.2×10^{-6} M s^{-1}. This value is approximately ten times smaller than the observed deperoxidation rate (*i.e.*, 1.1×10^{-5} M s^{-1}), thus indicating that reaction (4-8) is only a minor sink for $ROO^{\bullet}$ radicals (approximately 10%). Therefore, the rate limiting propagation reaction (4-7a) can be, in a good approximation, combined with two times the subsequent reaction (4-5) into a single overall chain propagation reaction (*i.e.*, $ROO^\bullet + ROO^\bullet$ (+ 2 ROOH) $\rightarrow$ 2 ROH + O_2 + 2 $ROO^\bullet$) with chain propagation rate (*i.e.*, $R_{prop} = k_{7a}[ROO^\bullet]^2$; a single chain involving two $ROO^\bullet$ chain propagators), but giving a rate of the ROOH removal by chain propagation (equation (4-9)):

$$(-d[ROOH]/dt)_{prop} = 2\ k_{7a}[ROO^\bullet]^2 \qquad (4\text{-}9)$$

According to this proposed mechanism (Scheme 4-1), the radical chain is not only propagated, but also terminated by two $ROO^\bullet$ radicals. Application of the radical steady state approximation, that is, equating the rate of chain initiation $R_{init} = k_1[Co^{II}][ROOH]$, to that of chain termination $R_{term} = k_{7b}[ROO^\bullet]^2$ leads to the expression (4-10) for the total ROOH removal rate: $-d[ROOH]/dt = (-d[ROOH]/dt)_{init} + (-d[ROOH]/dt)_{prop}$:

$$-d[ROOH]/dt = (3 + 2\ k_{7a}/k_{7b}) \times k_1 \times [Co^{II}] \times [ROOH] \qquad (4\text{-}10)$$

Thus, according to this chain mechanism, the experimentally observed rate coefficient $k(T)$ above is in fact $(3 + 2\ k_{7a}/k_{7b}) \times k_1$. The chain length, defined as the ratio of the chain propagation and chain termination rates, simply equals k_{7a}/k_{7b}. This ratio has been experimentally determined to be (7-10):1 for *tert*-butyl peroxyl radicals in benzene at 318 K.[49] A chain length on the order of 10, thus yielding $k(T) \approx 20 \times k_1$, appears reasonable, given that most of the nascent $RO^\bullet$ radicals produced in the mutual reaction of $ROO^\bullet$ will diffuse away from each other rather than combine. The temperature dependence of the k_{7a}/k_{7b} ratio is expected to be small as it is controlled by diffusion, thus meaning that the experimentally observed activation energy of 54 kJ mol^{-1} is a reasonable estimate for the energy barrier of the rate determining reaction.

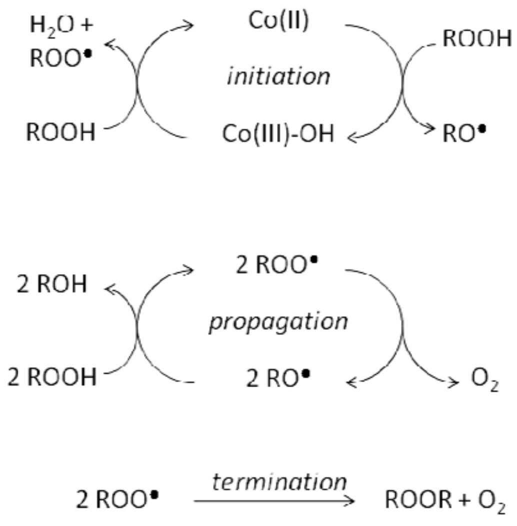

Scheme 4-1. The radical chain mechanism responsible for the Co^{II}-induced decomposition of ROOH.

It is important to emphasize that equation (4-10) correctly predicts the observed reaction orders for both cobalt and hydroperoxide. Many other mechanisms were considered, but all of them had to be rejected because they could either not explain the observed kinetics and/or the products observed in post-reaction analysis with gas chromatography (GC).

Under our conditions, the lifetime of ROOR is on the order of several days, that is, much longer than the timescale of the experiments. ROOR can thus be considered a true termination product. Experimental quantification of this compound, for example with GC, is very difficult given its low concentration and low stability in the GC injector (its lifetime at 473 K is only ≈ 1 s).

Although the general picture is clear and consistent, we have to return to the fate of the $Cy^•$ radicals formed in reactions (4-4) and (4-8). Despite our precautions to avoid O_2 in the system (by flushing the reactor with N_2), the formation of O_2 *in situ* cannot be avoided: about 0.5 O_2 is formed per ROOH consumed through reaction (4-7). Given that only approximately 0.15-0.2 $Cy^•$ radicals are expected to be generated per ROOH molecule removed, all $Cy^\bullet$ radicals will be able to react with O_2, thus yielding the $CyOO^\bullet$ radical. Indeed, with a diffusion controlled rate constant of 3×10^9 M^{-1} s^{-1}, the rate of $Cy^\bullet$ loss, even at [O_2] as low as 10^{-5} M, will still be as high as 3×10^4 s^{-1}, far higher than any other $Cy^\bullet$ radical reaction. Initially, at low ROOH conversions, the $CyOO^\bullet$ peroxyl radicals will react mainly with ROOH and *vice versa* (reaction (4-11)). This reaction is known to proceed with a rate constant of approximately 10^3 M^{-1} s^{-1} at 303 K in both directions.[46]

$$CyOO^\bullet + ROOH \leftrightharpoons CyOOH + ROO^\bullet \tag{4-11}$$

So, after a short time the two types of peroxyl radicals will be in (pre)equilibrium with [$CyOO^\bullet$] << [$ROO^\bullet$] given that [ROOH] >> [CyOOH]. Nevertheless, as the reaction proceeds, both $CyOO^\bullet$ and CyOOH will also start to react with the $ROO^\bullet$ radical and eventually also with cobalt, thus yielding cyclohexanol and cyclohexanone. However, the effective rate of CyOOH loss remains rather low due to its low concentration relative to ROOH, thus explaining why it can be detected by using GC. Significantly, the total amount of cyclohexane oxidation products observed with GC (*i.e.*, ± 15% with respect to *tert*-butyl alcohol) is in good agreement with the mechanism detailed above. This mechanism therefore also explains why the yield of the industrial deperoxidation of cyclohexyl hydroperoxide in cyclohexane exceeds 100% as one co-oxidizes a fraction of the cyclohexane solvent.

In summary, the mechanism shown in Scheme 4-1 is based on well characterized reactions (experimentally and/or computationally) and can not only explain the observed reaction rate and reaction orders, but also the minor fraction of cyclohexane oxidation products relative to the major product *tert*-butyl alcohol.

4.2.6 Mechanism at Higher Cobalt Concentrations

Although we seem to understand the chemistry at low cobalt concentrations, we are still faced with the challenge of rationalizing the very abrupt decrease of the deperoxidation rate observed once [Co(acac)$_2$] > 100 µM (Figure 4-6).

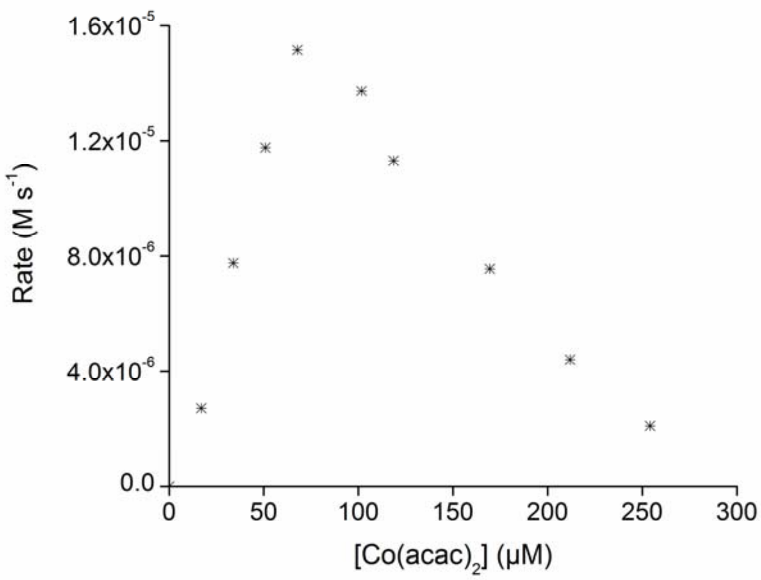

Figure 4-6. The observed rate of the decomposition of ROOH as a function of the total [Co(acac)$_2$] concentration; T = 333 K.

Inhibition at higher cobalt concentrations has been known for a long time and was often ascribed to the high oxidizing power of ROO$^\bullet$ radicals, assumed to form a stable complex with the Co^{II} catalyst:[3]

$$Co^{II} + ROO^\bullet \leftrightharpoons Co^{III}\text{-}OOR \tag{4-12}$$

Therefore, excessive Co^{II} ions would efficiently trap peroxyl radicals and hence interrupt the radical chain.[1, 3, 53] Although similar complexes have been synthesized,[54] the stability of the [Co(acac)$_2$]-OOR complex is probably insufficient to cause an irreversible removal of

$ROO^{\bullet}$ radicals. Indeed, although the complex is predicted to be stable for 82.4 kJ mol^{-1} at the UBP86/LANL2DZ level of theory, it is unstable at the UB3LYP/LANL2DZ level of theory. Given the opposite shortcomings of both consulted DFT functionals (*i.e.*, B3LYP and BP86), a moderate stability should be concluded (*i.e.*, between 0 and 84 kJ mol^{-1}). This peroxyl trapping mechanism can therefore only cause a leveling of the overall rate at increasing cobalt concentrations, but it cannot cause inhibition, that is, a net decrease of the rate. Instead, one would approach a constant reaction rate, independent of the total cobalt concentration. Note that in case such a Co^{III}-OOR complex would be infinitely strong (*i.e.*, even significantly stronger than predicted by UBP86/LANL2DZ), the catalyst would be irreversibly deactivated, which is in disagreement with the experimental observations (see above).

The sudden reversal of the dependence of the reaction rate on the cobalt concentration from a linear increase up to a value of $[Co(acac)_2] < 10^{-4}$ M to an abrupt decrease once $[Co(acac)_2] \geq 10^{-4}$ M is reached can only be explained by an additional and more efficient termination mechanism with the rate proportional to $[Co]^{\geq 2}$ but independent of $[ROO^{\bullet}]$. The latter condition is obvious: a dependence of the rate of the additional, faster termination mechanism on $[ROO^{\bullet}]$ would induce negative feedback because enhanced termination necessarily decreases $[ROO^{\bullet}]$. As already pointed out, irreversible deactivation of the catalyst on the timescale of our experiments can also be excluded because this behavior would cause a decrease of the observed rate constant as a function of time, which is not observed up to 50% conversion. This outcome implies that the cobalt species responsible for the enhanced termination must somehow be in steady state with the catalytically active cobalt species on the timescale of the experiments.

A hypothetical inhibition that is in line with the kinetic requirements above could thus involve [Co] in a reaction order ≥2. Various suggestions were made, but so far an unambiguous inhibition mechanism could not be proposed. A more detailed computational and experimental study on the cobalt speciation during the reaction conditions would most likely provide valuable insights in this inhibition mechanism.

4.3 Conclusion

Herein, the catalytic deperoxidation of *tert*-butyl hydroperoxide with [Co(acac)$_2$] was studied by *in situ* UV/Vis spectroscopic analysis at 323-343 K. It is proposed that a Fenton-type mechanism is responsible for the initiation of a radical chain mechanism propagated by alkoxyl and peroxyl radicals. The absence of an efficient termination channel in the mutual reaction of tertiary peroxyl radicals results in a chain length on the order of 10. The majority of the hydroperoxide radicals are therefore destroyed by propagation reactions rather than the Fenton-type cycle. At higher [Co(acac)$_2$] concentrations, strong inhibition of the radical chain is observed, thus causing a net decrease of the deperoxidation rate. This behavior can kinetically be explained with a termination reaction involving Co species in a reaction order ≥2. An unambiguous mechanism could though not be proposed. It is our aim to further characterize this reaction (both experimentally and computationally) and to investigate the influence of the ligands and additives. Also the performance of heterogeneous catalytic systems will be compared and rationalized in the light of the proposed mechanism.

4.4 Experimental Section

In the experimental set-up, the light of a deuterium-halogen source was guided by optical fibers to a magnetically stirred high pressure reactor (10 mL). The light was passed through the reactor (optical path length: ≈ 1 cm) through sapphire windows and guided to an Ocean Optics USB2000 spectrometer through a second optical fiber. The integration time of the

CCD detector was set at 5 ms, thus averaging out 100 spectra to improve the signal-to-noise ratio. A dark spectrum was recorded with a closed light shutter, while reference spectra were recorded with only cyclohexane in the reactor. The reaction was initiated by adding a known quantity of a pre-diluted *tert*-butyl hydroperoxide in cyclohexane (0.275 M) to an N_2-flushed solution of [Co(acac)$_2$] in CyH (5 mL) in the reactor, after which the reaction was monitored under an N_2 atmosphere. All the studied cobalt solutions were obtained from the same mother solution (1.0 mM [Co(acac)$_2$] in cyclohexane) through dilution with N_2-flushed cyclohexane. Note that the sapphire windows of the high pressure reactor absorb light below $\lambda \leq 220$ nm, thus deforming the far-UV range of the spectrum.

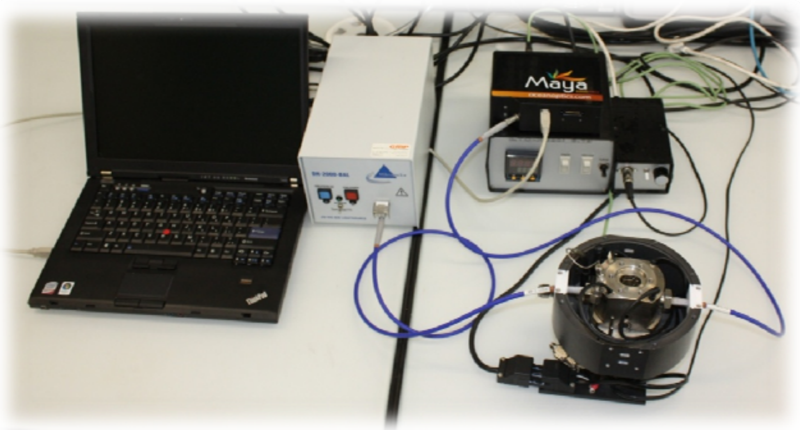

Figure 4-7. Experimental set-up for *in situ* UV/Vis measurements.

Quantum-chemical calculations were performed with the Gaussian03 software[55] at the indicated level of theory. The reported relative energies of the stationary points on the potential energy surfaces (*i.e.*, energy barriers E_b and reaction energies $\Delta_r E$) were corrected for ZPE differences.

5

HETEROGENEOUS CATALYSIS

The aerobic oxidation of cyclohexane was studied at 130 °C in the presence of a Co/SiO_2 catalyst, synthesized by flame spray pyrolysis. Characterization of the material indicates that at low Co loadings, Co^{II} is predominantly present as tetrahedral species, whereas at higher loadings also small amounts of octahedral species can be found at the surface of the agglomerated nanoparticles. Catalytic experiments demonstrate high activity, causing a complete *in situ* deperoxidation of the intermediate cyclohexyl hydroperoxide. Hot separation and catalyst recycle tests corroborate the heterogeneous nature of the catalyst.

5.1 Introduction

As seen in sections 1.2.2 and 4.2.5, cobalt ions take over the role of cyclohexyl peroxyl ($CyOO^{\bullet}$) radicals in the consumption of cyclohexyl hydroperoxide (CyOOH). A Fenton-type mechanism is generally assumed to take place. This catalytic cycle does not only decrease the CyOOH concentration, it also speeds up the rate determining initiation reaction (*i.e.*, the formation of radicals), explaining why the reaction temperature can be lowered. However, this simple mechanism fails to explain, for instance, why at higher cobalt concentrations, the reaction is inhibited (see section 4.2.6).

The use of homogeneous deperoxidation catalysts causes several (technical) limitations. One of them is that the catalyst cannot be recycled and ends up in a high boiling waste stream. Another problem is that one is restricted to low catalyst concentrations in order to minimize contamination of the waste, and to prevent the deposition of cobalt to the stainless steel reactor walls. For these reasons, it would be of interest to develop a solid (heterogeneous) catalyst for this reaction. In the literature, a multitude of materials have already been proposed,[*e.g.*, 56-60] and providing an overview of all those systems would be beyond the scope of this chapter. However, from a strategic (engineering) point of view, the following thoughts can be made. Many of the reported catalysts are high surface area materials, featuring active sites which are located in (micro/meso)pores. Given the detrimental effect of mass transfer limitation on the selectivity towards products which can react further (as is the case with desired partial oxidation products), and the increased polarity of the oxygenated products compared to the substrate, one can wonder if immobilization in microporous materials is an optimal approach. On the other hand, a high surface area is often required to achieve a high dispersion (accessibility) of the transition metal sites. One approach which some of us proposed a while ago is the immobilization of chromium hydroxy oxide colloids to the external surface of a silica support *via* a process called column precipitation chromatography (CPC).[61, 62] This technique combines the synthesis of small particles with their *in situ* immobilization, preventing sintering. An alternative approach that we report in this chapter, is the synthesis of nano-structured particles of cobalt-containing silica with flame spray pyrolysis (FSP). FSP is a convenient technique to synthesize thermally stable materials with interesting properties as solid catalysts. Additional advantages of these materials is that they provide a high surface area without micropores, and that the synthesis is highly reproducible and scalable.[63-66]

5.2 Experimental

5.2.1 Synthesis of the Nanostructured Co/SiO_2 Particles

Nanostructured Co/SiO_2 particles were made by flame spray pyrolysis (FSP) of appropriate precursor solutions. Cobalt(II) 2-ethylhexanoate (Co-2-ethylhexanoate, 12% Co, STREM Chemicals) and hexamethyl disiloxane (HMDSO, Aldrich, >98%) were used as cobalt and silicon precursors, respectively, dissolved in xylene (Riedel-de Haën, >96%) and 2-ethylhexanoic acid (Riedel-de Haën, >99%) in a ratio of 2:3, resulting in a total metal concentration of 1 mol L^{-1}. This precursor solution was fed by a syringe pump through the FSP nozzle and dispersed by O_2 (Pan Gas, 99.95%, 5 L min^{-1}) into a fine spray that was ignited and sustained by a premixed CH_4/O_2 flame. Additional 5 L min^{-1} of sheath O_2 was fed in the reactor through a metal ring (11 mm internal diameter, 18 mm outer diameter) with 32 holes (0.8 mm internal diameter) to ensure complete combustion (Scheme 5-1). A detailed description of the laboratory scale FSP reactor can be found elsewhere.[67] The powders were collected with the aid of a vacuum pump (Busch SV 1050 B) on a glass microfiber filter (Whatman GF/D, 257 mm in diameter).

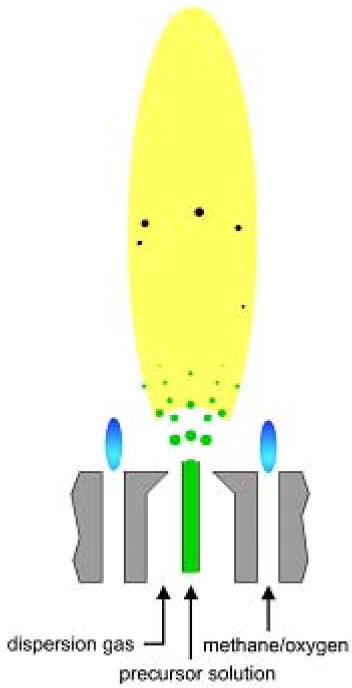

Scheme 5-1. Flame spray pyrolysis (FSP) set-up for the production of nanostructured Co/SiO_2 particles.

5.2.2 Characterization

The specific surface area (m^2 g^{-1}) of the materials was determined by nitrogen adsorption (Pan Gas, >99.999%) at 77 K by the Brunauer–Emmett–Teller (BET) method with a Micromeritics Tristar 3000 (five point isotherm, $0.05 < p/p_0 < 0.25$). The Co loading of the material was determined with ICP-OES (Horiba, Ultima 2) after digestion with HF and found in fair agreement with the composition of the precursor solution. Raman spectra were recorded with a Renishaw InVia Raman microscope with a 514 nm laser excitation (≈1 mW). Infrared spectra were recorded with a Bruker Vertex 70 V spectrometer (LN-MCT Mid detector) in a Pike Miracle® attenuated total reflectance (ATR) cell with a diamond crystal, or with a Bruker Alpha-P FT-IR spectrometer equipped with a diffuse reflectance module (DRIFT) mounted inside a glove box; KBr was taken as background for the DRIFT spectra. Diffuse reflectance (DRS) UV/Vis spectra were recorded with an Ocean Optics Maya 2000Pro spectrometer with a backscatter probe; in order to obtain Kubelka-Munk values below 1 and reproducible reflectivities, the samples were diluted in $BaSO_4$ as mentioned in the text and measured against a $BaSO_4$ background.

5.2.3 Catalytic Experiments

The experiments were performed at 130 °C in a 100 mL 316 stainless steel autoclave, equipped with an inert Polyether Ether Ketone (PEEK) insert, including a PEEK top lid, PEEK stirrer and a PEEK covered thermocouple. The short heating time (15 min) and the accurate temperature control ensured stable conditions during the reaction. After loading the reactor with catalyst and cyclohexane (30 mL), 400 psi (*i.e.*, 27.6 bar) of oxygen pressure (Pan Gas 99.999 vol%) was added to the reactor, prior to heating. Notice that a potentially explosive gas mixture is formed. Therefore, the reactor vessel was connected to a steel expansion vessel of 20 L *via* a rupture disk, designed to open at 207 bar. The pressure in the reactor was monitored with a pressure gauge and a pressure sensor (Keller), connected to a computer. Slurry samples were withdrawn from the reactor *via* a PEEK sampling tube and analyzed by GC (HP6890; HP-5 column, 30 m/0.32 mm/0.25 mm; Flame Ionization Detector). Biphenyl was added to the cyclohexane in 0.25 mol%, and used as an inert internal standard for product quantification. In order to ensure that all insoluble/adsorbed by-products were also quantified, the withdrawn samples were centrifuged, the solid catalyst washed 3× with acetone, and the solutions combined. The O-H groups in the reaction mixture were silylated with *N*-methyl-*N*-(trimethylsilyl)trifluoroacetamide (MSTFA) to facilitate the separation of the alcohol and the ketone product; note that the acidic by-products such as adipic and glutaric acid are also silylated by MSTFA. The hydroperoxide yield was determined *via* a double injection into the GC, with and without reduction of the reaction mixture by trimethylphosphine (Sigma-Aldrich, 1 M in toluene), prior to silylation. From the obtained augmentation in alcohol content, the corresponding hydroperoxide yield was determined. Product identification was done with GC-MS with cool-on-column injection to prevent thermal dissociation in the GC liner.

5.3 Results and Discussion

5.3.1 Flame-Made Co/SiO_2

Using flame spray pyrolysis (FSP), Co/SiO_2 materials were synthesized with various amounts of cobalt, ranging from 3.4 to 7.6 wt%. Previously, the FSP method was demonstrated to be very reproducible.[68] The actual Co content, measured by ICP-OES after digestion with HF, and the BET surface areas of the materials are summarized in Table 5-1.

Table 5-1. Specific surface area of the various FSP-made Co/SiO_2 materials.

entry	catalyst loading (wt%)[a]	specific surface area according to BET ($m^2\ g^{-1}$)
a	3.4	330
b	4.8	300
c	5.6	270
d	7.6	220

[a] Determined by ICP-OES after complete digestion in HF (absolute error margin estimate at ±1%).

Flame-made silica particles from turbulent, vapor-fed flames are known to have an agglomerate size of around 10-300 nm,[69] the structure of the agglomerates being very fractal (D_f around 2.1).[70] FSP-made silica-based materials usually show a type IV isotherm with a very small hysteresis loop and possess no micro- or mesoporosity as seen for

Pt/SiO_2[68] and V_2O_5/SiO_2[71] catalysts. Doping silica with Co has a pronounced effect on the specific surface area: starting from around 270 m^2 g^{-1} for pure FSP-made SiO_2 (not shown), the surface area initially increases for the 3.4 wt% sample up to around 330 m^2 g^{-1}. Increasing the Co content further decreases the specific surface area even below the value of pure SiO_2. A similar trend of maximum specific surface area at low dopant content has already been observed previously for FSP-made Ta_2O_5/SiO_2,[72] V_2O_5/SiO_2,[71] ZnO-containing SiO_2[73-76] and $Cs_2O/Pt/Al_2O_3$.[68] In these studies it was shown by means of ammonia temperature programmed desorption (TPD) that the particle surface is enriched with the doping element and is significantly different from pure FSP-made silica[72] or alumina,[71] respectively. Therefore, the initial increase in surface area (*i.e.*, from 270 to 330 m^2 g^{-1} for 0-3.4 wt% cobalt) could be related to an influence of the cobalt constituent on the SiO_2 sintering rate and corroborates Co enrichment on the particle surface rather than incorporation in the bulk. The subsequent decrease in surface area at higher Co contents may be attributed to a segregation of CoO_x clusters reducing the effect on the sintering rate and leading to larger primary particles and at higher contents, segregation of the dopant-metal-oxide reducing the overall specific surface area as observed for Ta_2O_5/SiO_2[72] and V_2O_5/SiO_2.[71]

The UV/Vis diffuse reflectance (DRS) measurements of the different materials are reported in Figure 5-1. Around 600 nm, one observes the typical triplet band, characteristic for isolated, tetrahedrally coordinated Co^{II} (assigned to the $^4A_2(F) \rightarrow {}^4T_1(P)$ transition).[77] In addition, one observes an increased intensity around 400-550 nm for the 7.6 wt% sample, probably due to octahedrally coordinated cobalt ions.[75-77] (As a comparison, Figure 5-1 also shows the DRS spectra of Co_3O_4 and CoO.) Note that the prominent presence of tetrahedral Co^{II} species corroborates the surface enrichment hypothesis as incorporation of cobalt in the silica bulk would require charge compensating cations like protons being incorporated in the bulk silica (*viz.* substitution of Co^{II} for Si^{IV}).

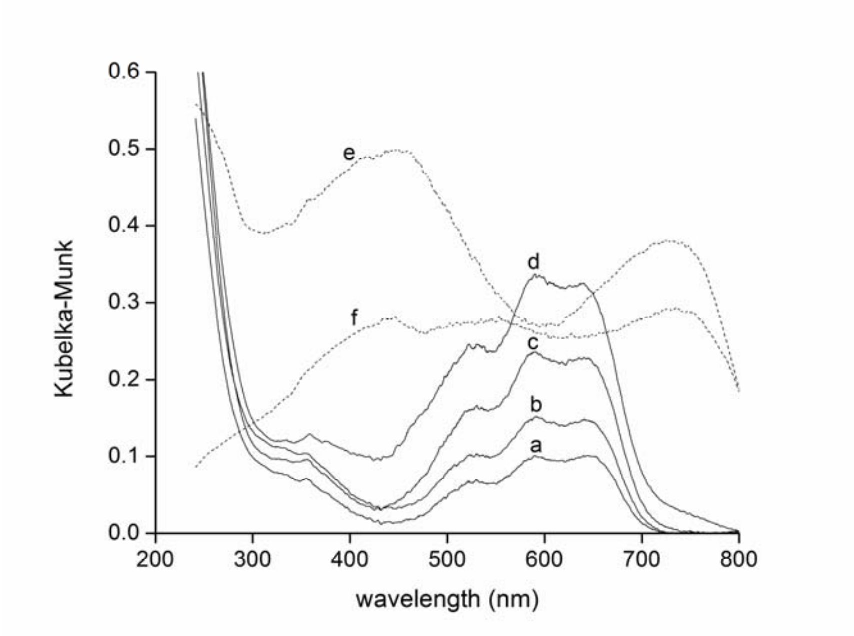

Figure 5-1. DRS spectra of the FSP-made Co/SiO_2 samples (a-d, see Table 5-1; diluted 1:9 in $BaSO_4$), and of Co_3O_4 (e) and CoO (f; diluted 1:40 and 1:8, respectively, in $BaSO_4$).

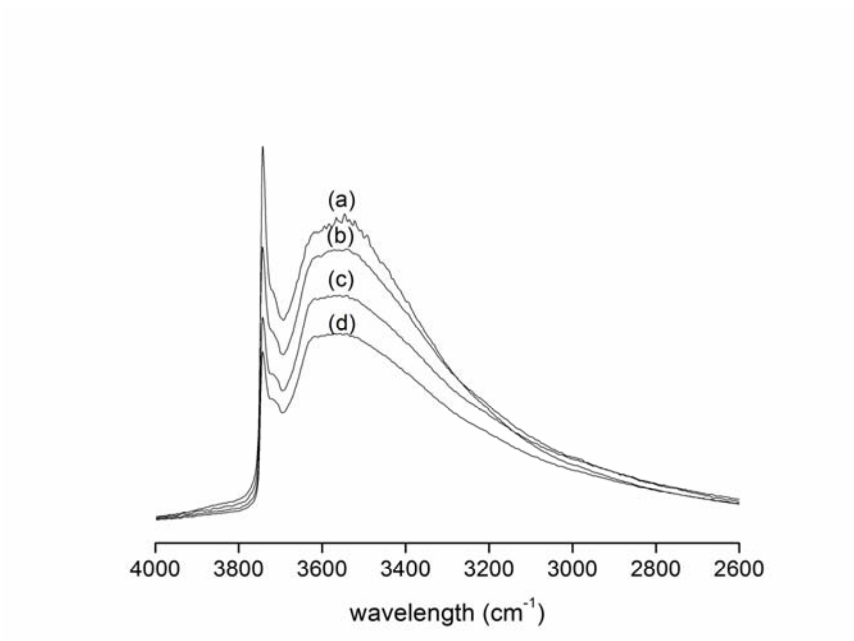

Figure 5-2. DRIFT spectra of the different Co/SiO_2 samples (a-d, see Table 5-1).

Diffuse reflectance infrared Fourier transform (DRIFT) spectroscopy shows a broad band corresponding to hydrogen-bonded silanol vibrations around 3560 cm^{-1} and a sharp peak at 3740 cm^{-1} corresponding to isolated SiOH surface species; both signals decrease at increasing Co loadings, indicating that the cobalt influences the silica surface significantly. IR spectroscopy also reveals that no residual organic species can be found on the fresh materials (which could originate from incomplete combustion of the precursor solution) (Figure 5-2).

Raman spectroscopy shows several features (Figure 5-3), and the most significant change is the growing signal at ≈680 cm^{-1} with increasing Co loadings, probably due to the formation of cobalt oxides at increasing loadings. This observation is consistent with the DRS spectra in Figure 5-1, providing evidence for octahedrally coordinated species at higher Co loading and corroborates the hypothesis of CoO_x segregation from BET analysis (*vide supra*). However, as the extinction coefficient of octahedral cobalt is lower than of tetrahedral cobalt (d-d transitions are symmetry forbidden),[75-77] those higher coordinated species are barely visible with UV/Vis spectroscopy.

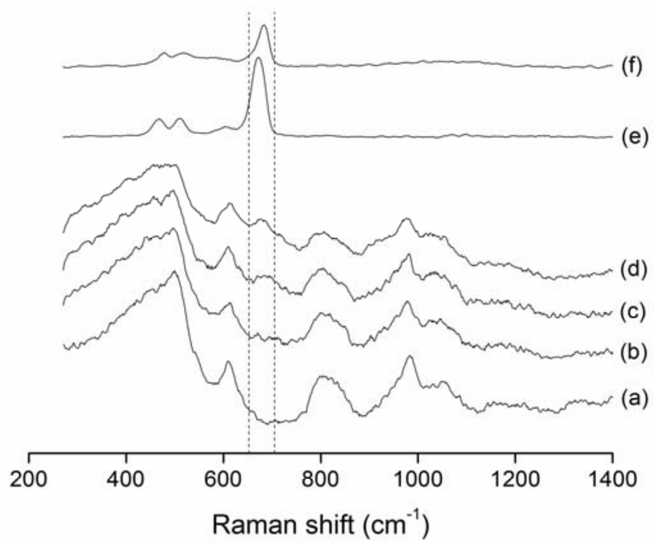

Figure 5-3. Raman spectra of the different Co/SiO_2 materials (a-d, see Table 5-1), Co_3O_4 (e) and CoO (f).

Summarizing the characterization results, one can conclude that cobalt is predominantly present as isomorphously substituted Co^{II} ions in a tetrahedral environment, mainly on the particle surface. Only at high Co loadings, octahedrally coordinated cobalt species are detected with UV/Vis and Raman spectroscopy, presumably present as very small cobalt oxides.

5.3.2 The Catalytic Performance

The performance of the FSP-made Co/SiO_2 materials as a catalyst for cyclohexane oxidation was studied at 130 °C under 400 psi (*i.e.*, 27.6 bar) pure oxygen (room temperature pressure, *i.e.*, prior to heating). Under those conditions, the thermal (*i.e.*, the uncatalyzed) activity is negligible in the investigated timeframe. The catalytic activity (Figure 5-4) appears to be significantly higher than that of commercially available Co_3O_4 nano-particles (Sigma-Aldrich, size <50 nm), and much higher than the activity of the uncatalyzed system. To our initial surprise, the activity and selectivity are nearly independent of the Co loading (see for instance Figure 5-4). This effect can either be due to a constant amount of accessible and catalytically active sites at the surface of the materials, independent of the Co loading, or, and more probable, due to a saturation effect. It was indeed observed that 5 ppm of the 3.4 wt% Co/SiO_2 performed equally well as 25 ppm of the same material. Apparently, once a critical amount of active Co sites is present, further increase of the catalyst concentration does not increase the performance. It is possible that a change in rate determining step from CyOOH coordination/diffusion to the Co sites to the actual decomposition at the active site, is behind this observation. However, more kinetic experiments are required to verify this hypothesis.

Of practical interest is the very low CyOOH selectivity (Figure 5-5), compared to the thermal autoxidation (Figure 5-6).

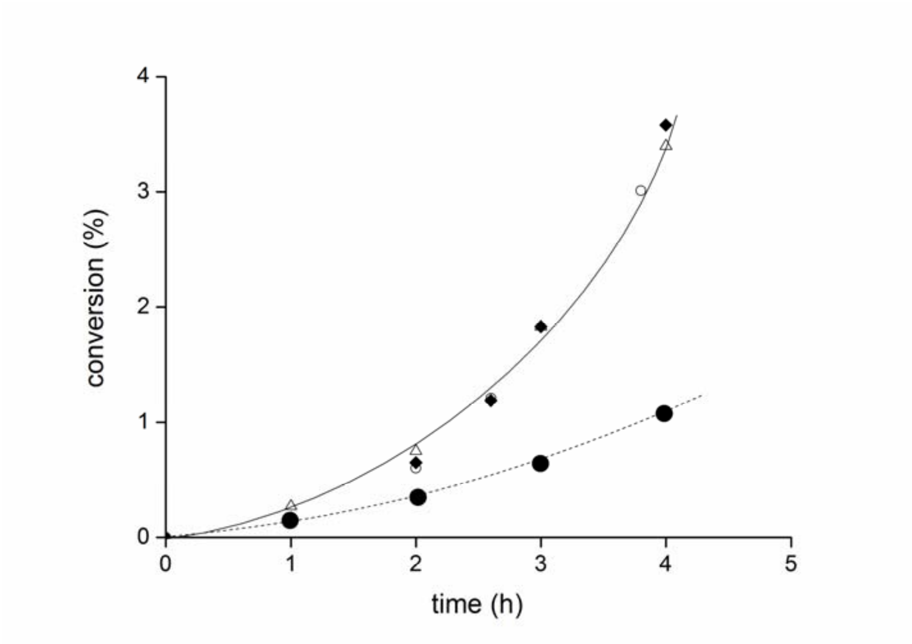

Figure 5-4. Evolution of the cyclohexane conversion as a function of time at 130 °C using 25 mg L^{-1} cobalt, using various catalysts: 3.4 wt% Co/SiO_2 (*filled diamond*), 4.8 wt% Co/SiO_2 (*open circle*), 7.6 wt% Co/SiO_2 (*open triangle*), and Co_3O_4 nanoparticles (*filled circle*, <50 nm, Sigma-Aldrich).

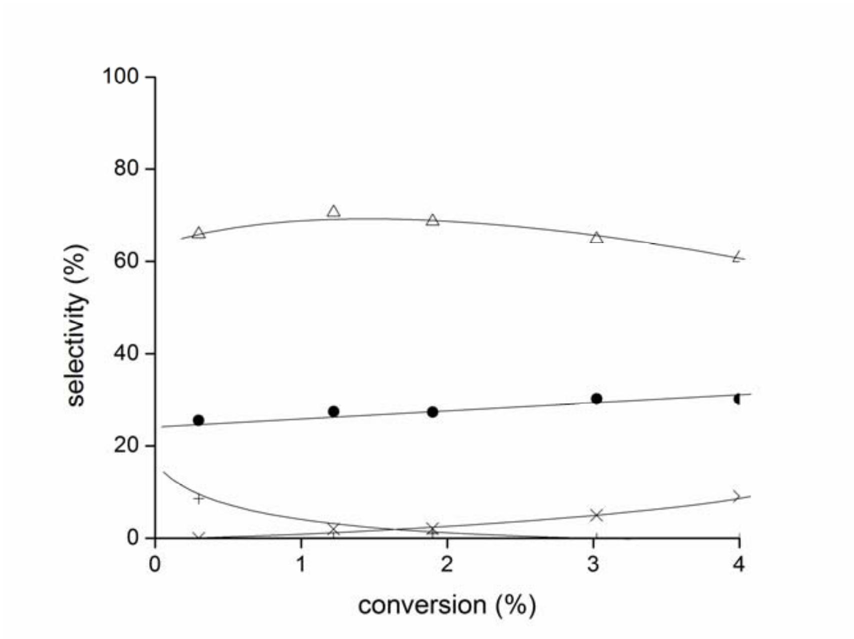

Figure 5-5. Product distribution obtained during a catalytic cyclohexane oxidation experiment at 130 °C, using 25 ppm of a 3.4 wt% Co/SiO_2 sample: CyOOH (*plus)*, CyOH (*open triangle*), Q=O (*filled circle*) and by-products (*cross*, sum of 6-hydroxyhexanoic acid, 6-hydroperoxyhexanoic acid, adipic acid, glutaric acid and ε-caprolactone).

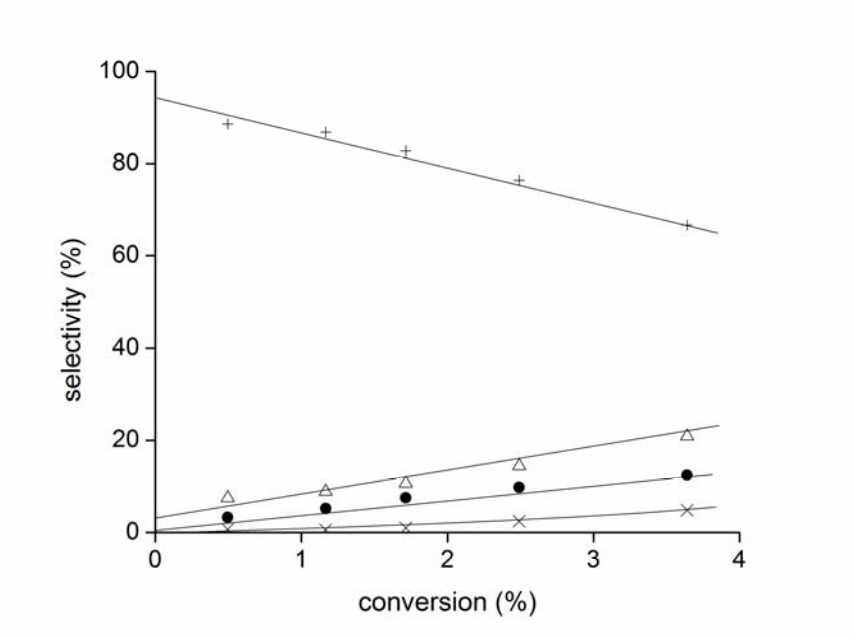

Figure 5-6. Product distribution obtained during a pure autoxidation experiment at 145 °C: CyOOH (*plus*), CyOH (*open triangle*), Q=O (*filled circle*) and by-products (*cross*, sum of 6-hydroxyhexanoic acid, 6-hydroperoxyhexanoic acid, adipic acid, glutaric acid and ε-caprolactone).

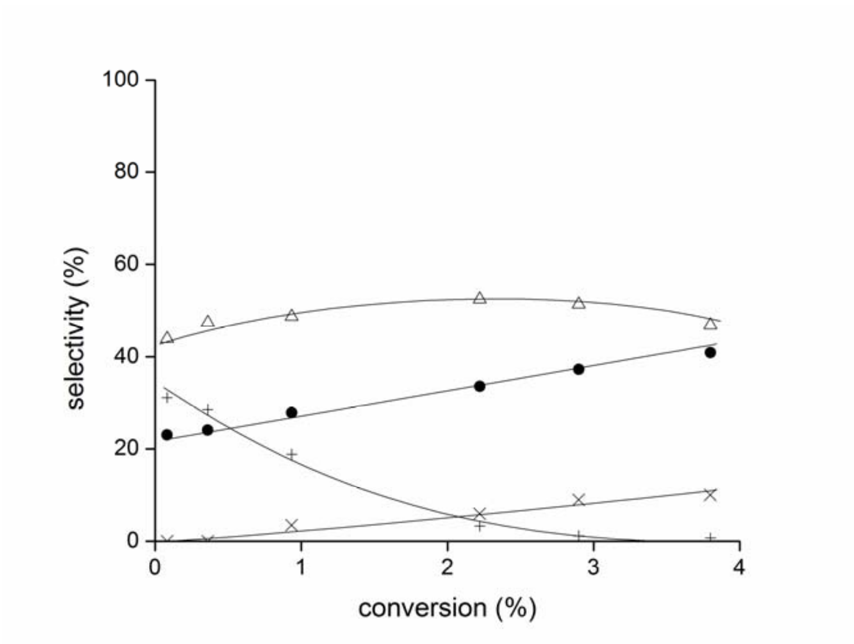

Figure 5-7. Product distribution obtained during a catalytic cyclohexane oxidation experiment at 130 °C, using 5 ppm of $Co(acac)_2$: CyOOH (*plus*), CyOH (*open triangle*), Q=O (*filled circle*) and by-products (*cross*, sum of 6-hydroxyhexanoic acid, 6-hydroperoxyhexanoic acid, adipic acid, glutaric acid and ε-caprolactone).

Figure 5-7 shows the selectivity as a function of the conversion for a cyclohexane oxidation, catalyzed by 5 ppm Co(II) acetylacetonate – $Co(acac)_2$ – which features a similar activity as the reported heterogeneous systems.[78] However, the use of such a high concentration of a homogeneous catalyst is technically prohibited (see section 5.1). Remarkable is that the heterogeneous catalyst results in a higher CyOH yield, due to a more complete deperoxidation. Possibly this can be attributed to sorption effects, increasing the local CyOOH concentration near the catalytic sites.

5.3.3 Coordination of Hydroperoxide

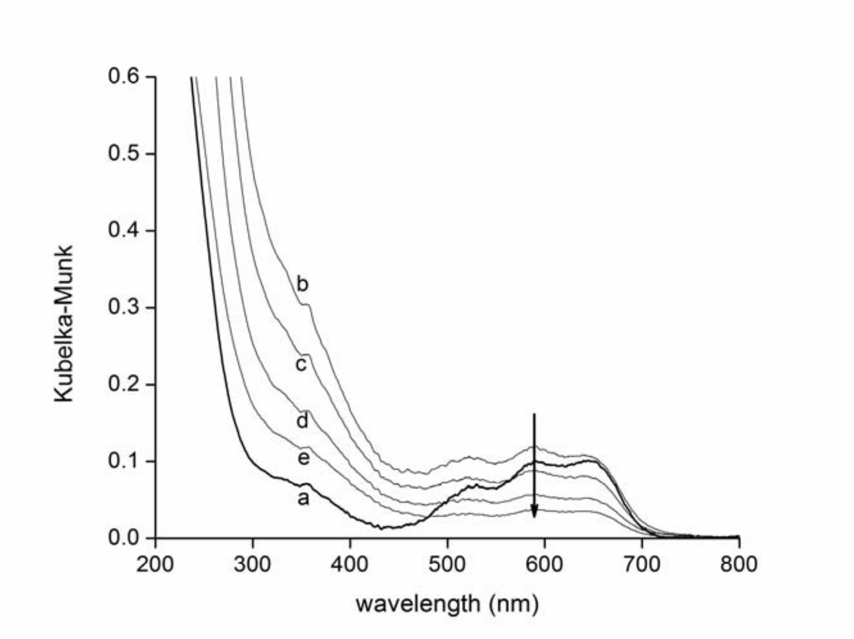

Figure 5-8. DRS spectra of the 3.4 wt% FSP Co/SiO_2 material, before (a), and after (b) exposure to a 100 mM *tert*-butyl hydroperoxide solution; spectra (c-e) were recorded at 5 minutes time interval.

When the catalyst is impregnated with a 100 mM *tert*-butyl hydroperoxide solution (diluted in cyclohexane), the broad triplet band around 600 nm in the DRS spectrum decreases significantly in intensity (Figure 5-8). (The increased UV-signal can be attributed to the absorption by the hydroperoxide itself.) Note that this observation supports the hypothesis that the tetrahedral Co^{II} species are located at the surface of the material, accessible for reactants. Indeed, probably this means that the hydroperoxide is coordinating, breaking the tetrahedral symmetry of the cobalt sites. More (*in situ*) spectroscopic work is required to verify if this observation implies that the active deperoxidation site is a [CoO_4] surface species.

5.3.4 Product Analysis and Desorption of By-Products

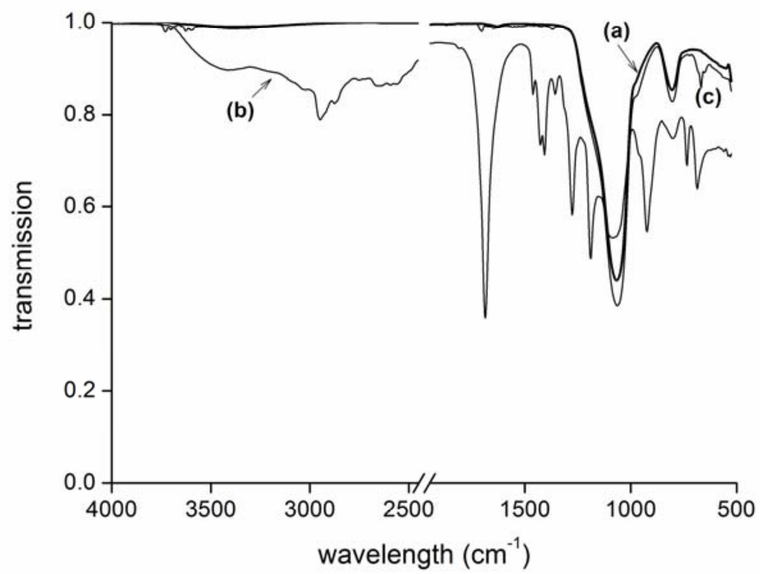

Figure 5-9. Attenuated total reflection IR spectra of the 3.4 wt% Co/SiO_2 before a catalytic run (spectrum a), after a catalytic run (spectrum b), and after subsequent washing with acetone (3×, spectrum c).

Important to emphasize here is the need for a quantitative product analysis.[79] Indeed, after a catalytic run, a lot of by-products such as adipic acid are adsorbed to the solid catalyst. Attenuate total reflection infrared (ATR-IR) spectroscopy actually only detects adipic acid (Figure 5-9). As a consequence, it is very easy to overestimate the selectivity.

Indeed, in case of inhomogeneous sampling (*i.e.*, only liquid is sampled, no solid material containing adsorbed by-products), or if the catalyst is not carefully washed with acetone to dissolve the by-products for correct product quantification (see section 5.2.3), a much higher selectivity was observed, surpassing the current state-of-the-art (Figure 5-10). The ATR-IR results in Figure 5-9 show that the adipic acid can indeed be desorbed from the solid catalyst upon washing with acetone. This analytical procedure results in a similar overall selectivity towards the sum of desired products as the uncatalyzed thermal autoxidation reaction, however with a negligible contribution of CyOOH.

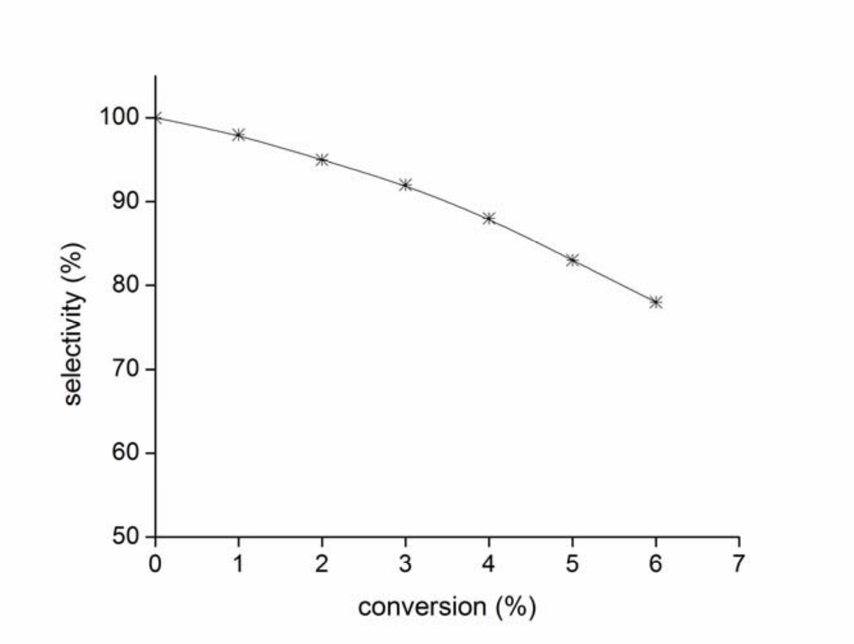

Figure 5-10. Evolution of the overall selectivity versus the conversion for a thoroughly analyzed cyclohexane autoxidation system.

5.3.5 Stability of the Catalyst: Hot Separation Test

A common problem encountered in liquid phase applications of solid catalysts is leaching of the active elements. Especially for (aut)oxidation reactions, leaching is a notorious issue.[40a] One of the most robust lab-scale experiments to verify if leached species cause homogeneous rather than heterogeneous catalysis, is the so-called hot separation test. In this experiment, the supernatant is separated from the solid catalyst (*e.g.*, by centrifugation), prior to cooling down of the reaction mixture. Indeed, the latter could induce readsorption or reprecipitation of leached species. Subsequently, the remaining activity of the supernatant devoid of catalyst is examined under the same conditions. In case that the catalysis is purely caused by leached species, the oxygenation activity of the supernatant would match the activity of the catalytic (slurry) system (under the assumption that there is no important support effect, boosting the activity). In our case, a hot reaction mixture containing the solid catalyst (3.4 wt% Co/SiO_2) was centrifuged after 2.5 h, and the oxidation of the supernatant was followed for another 2 h. As can be seen from Figure 5-11, the conversion did continue to increase, albeit at a much lower rate. Previously, a very similar behavior was observed in a hot separation test of supported chromium nano-particles.[61, 62] The persistence of a low activity can be attributed to the thermal autoxidation, initiated by the oxygenated products, present in the supernatant.[61, 62] An important observation is that the CyOOH selectivity in the supernatant increases very rapidly, *i.e.*, from nearly zero in the catalytic slurry system (see Figure 5-5) to 20% in the supernatant test after 2 h of reaction (*viz.* at 2% conversion, see Figure 5-11). This observation provides strong evidence to assume that no catalytically active amounts of cobalt are leached in solution as this would keep the CyOOH selectivity very low indeed. Similar results were observed if the hot separation test was performed after 3.5 h. The cobalt concentration in the supernatant solution was also investigated by ICP-OES and found to be below the detection limit, implying that less than 1% of the cobalt could have leached out without noticing it.

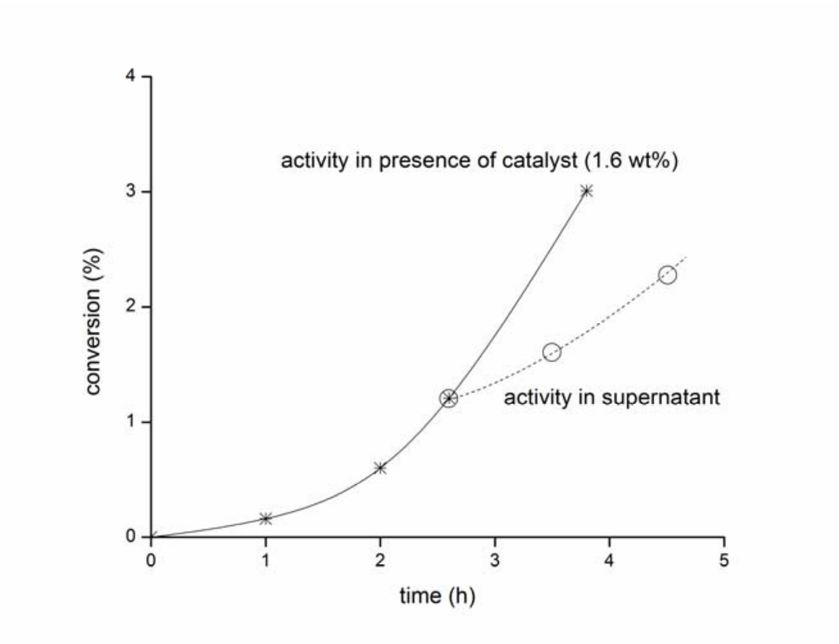

Figure 5-11. Results of a hot separation test at 130 °C: the solid catalyst (25 ppm, 3.4 wt% Co/SiO_2) is separated from the hot reaction mixture after 2.5 h and the conversion of the supernatant monitored for an additional 2 h.

Recycling of the FSP Co/SiO_2 catalyst has also been examined under the usual conditions (27.6 bar O_2, 130 °C). After a 4 h oxidation run, the solid catalyst (3.4 wt%, 25 ppm) was separated from the liquid phase and washed several times with acetone to remove adsorbed by-products (*vide supra*). Subsequently the solid was dried at 70 °C in a vacuum oven. The reaction rate with the recycled catalyst was slightly higher than with fresh catalyst, probably due to the presence of small amounts of organic products which were not completely removed upon washing (see Figure 5-9, spectrum c). However, the two subsequent recycle experiments all showed the same steady activity. It is important to emphasize that the product distributions remained essentially the same during these recycle experiments. All these results hence point towards the heterogeneous nature of this FSP Co/SiO_2 catalyst.

5.4 Conclusion

Flame spray pyrolysis was used as a convenient technique to synthesize Co/SiO_2 materials with different loadings. At low loadings, the cobalt is mainly present as tetrahedral species at the surface of the particles. At higher loadings, also octahedral cobalt, probably (mixed) cobalt oxide, can be detected by DRS UV/Vis and Raman spectroscopy. The materials were demonstrated to be active autoxidation catalysts, affording very low hydroperoxide selectivity. This does not only improve the intrinsic safety of the oxidation process, but it also eliminates the need for a second, subsequent deperoxidation step. Emphasis is put on correct product analysis to study the intrinsic selectivity of the system; leaching of active cobalt species which could cause homogeneous rather than heterogeneous catalysis can be neglected, based on hot separation and recycle experiments. In subsequent work, the long term stability of the catalyst under continuous flow conditions should be investigated.

OUTLOOK

During these doctoral studies several steps have been made towards a better understanding of the autoxidation mechanism. After the addition of (di)unsaturated molecules to the thermal autoxidation, an increased reaction rate could be quantified and confirmed with computational methods, pointing to an enhanced initiation *via* a bimolecular mechanism. Through UV/Vis measurements of the deperoxidation of the model peroxide (*i.e.*, *tert*-butyl hydroperoxide) a mechanism could be proposed which explains the positive correlation of the deperoxidation rate and the amount of dissolved Co catalyst. At higher catalyst concentrations, however, a net decrease of the reaction rate was observed. The hypothesis put forward is that Co dimers or oligomers are responsible for the reaction inhibition. An unambiguous mechanism could though not be proposed. A way of testing if cobalt in a higher reaction order is involved in this inhibition is *via* a heterogeneous catalyst which oviously cannot form any dimers being immobilized on the support. For this purpose, Co/SiO_2 nanostructured particles made by flame spray pyrolys (FSP) were used under high pressure conditions and showed an activity for the autoxidation of cyclohexane similar to that using the homogeneous catalyst Co(II) acetylacetonate. Surprisingly, the product distribution and the conversion were not affected by the Co loading; neither a deceleration was observed at higher cobalt concentration.

Keeping these improvements and findings in mind, one should consider further experiments which would lead to more molecular insights. For example, the influence of additives could be investigated during the catalytic autoxidation. Some preliminary experiments showed that the addition of ketone to the reaction mixture enhances the reaction rate; alcohol, however, seems to slow down the reaction (see Figure O-1). A mixture of both additives apparently cancels out its effect. The rate acceleration seems to be correlated to the additive concentration. Further experiments at different temperatures, considering the use of several oxygenated additives, could lead to quantification of the energy barriers and improve the proposed reaction mechanism.

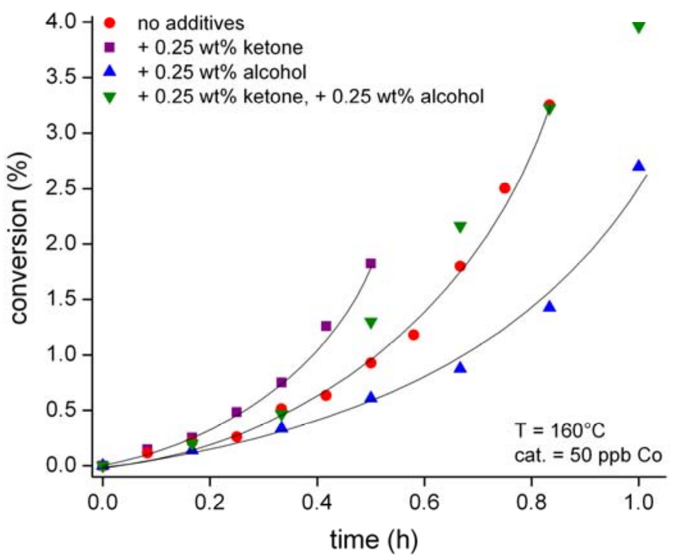

Figure O-1. Catalytic autoxidation of cyclohexane in presence of 50 ppb Co(II) 2-ethylhexanoate in solution at 160 °C upon addition of different amounts of oxygenated molecules.

Bulky ligands in homogeneous catalysts might hinder molecules from reacting with each other and possibly inhibit the propagation. Testing various complexes with different ligands and/or metal ions would help understanding the behavior of the acting species and the catalytic cycles.

The positive results using FSP made particles encourage the investigation of the autoxidation reaction with particles made of different metal ions. Considering the stability of the catalyst, also the use of a fixed bed plug flow reactor could be tested. Keeping the retention time low enough, the conversion would not exceed 5%; the amount of by-products, and consequently also its adsorption on the heterogeneous catalyst, could thus be minimized.

Microstructured reactors could also be used for the kinetic investigation of the autoxidation and the deperoxidation reactions. The small scale would have the advantages of excellent heat and mass transfer. Changing the flow rates, the retention times could be adapted to the desired conversion, improving the selectivity. Higher rates could be achieved due to higher operation temperatures without causing safety problems.

Interesting would be to analyze the heterogeneous catalyst in contact with the substrate *in situ*. This would give some insights on the formed (active) species at the solid-liquid interface.

A

SUPPORTING INFORMATION TO CHAPTER 4

A.1 Calibration Curve *tert*-Butyl Hydroperoxide

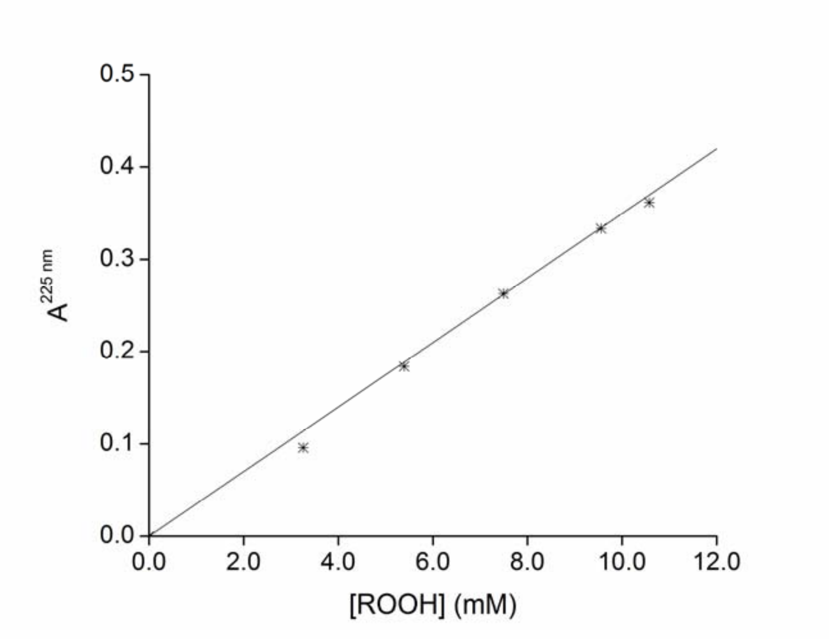

Figure A-1. Calibration curve of *tert*-butyl hydroperoxide in cyclohexane: absorbance at 225 nm versus concentration. The linear response curve (correlation coefficient R = 0.9995) supports the predominant presence of monomer ROOH species (see text).

A.2 $Co(acac)_2$ Spectra in Cyclohexane

Note that the intense 280 nm signal of $Co(acac)_2$ in Figure A-2 is linear in $[Co(acac)_2]$ up to 150 µM or an absorption value of ≈1.8. At higher concentrations, as expected, significant deviation from the Lambert-Beer law occurs.

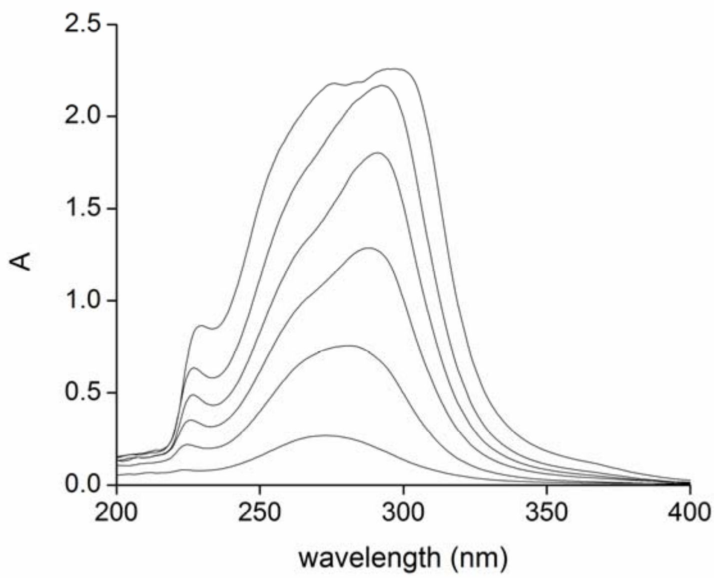

Figure A-2. Absorbance spectra of $Co(acac)_2$ solutions in cyclohexane (17, 50, 85, 120, 170 and 254 µM) at 333 K.

REFERENCES

[1] G. Franz, R. A. Sheldon, *Oxidation*, *Ullmann's Encyclopedia of Industrial Chemistry*, Wiley-VCH, Weinheim, **2000**.

[2] K. K. Rohatgi-Mukherjee, *Fundamentals of Photochemistry*, New Age International Ltd, New Delhi, **1978**.

[3] R. A. Sheldon, J. K. Kochi, *Metal-Catalyzed Oxidations of Organic Compounds*, Academic Press, New York, **1981**.

[4] H. L. J. Bäckström, *J. Am. Chem. Soc.* **1927**, *49*, 1460.

[5] B. Criegee, H. Pilz, H. Flygare, *Ber. Dt. Chem. Ges.* **1939**, *72*, 1799.

[6] E. H. Farmer, *Rub. Chem. Techn.* **1942**, *15*, 756.

[7] I. Hermans, T. L. Nguyen, P. A. Jacobs, J. Peeters, *ChemPhysChem* **2005**, *6*, 637.

[8] I. Hermans, P. A. Jacobs, J. Peeters, *J. Mol. Catal. A: Chem.* **2006**, *251*, 221.

[9] L. Vereecken, T. L. Nguyen, I. Hermans, J. Peeters, *Chem. Phys. Lett.* **2004**, *393*, 432.

[10] I. Hermans, J. Peeters, L. Vereecken, P. Jacobs, *ChemPhysChem* **2007**, *8*, 2678.

[11] I. Hermans, J. Peeters, P. Jacobs, *J. Org. Chem.* **2007**, *72*, 3057.

[12] I. Hermans, P. A. Jacobs, J. Peeters, *Chem. Eur. J.* **2007**, *13*, 754.

[13] I. Hermans, P. A. Jacobs, J. Peeters, *Chem. Eur.J.* **2006**, *12*, 4229.

[14] M. T. Musser, *Cyclohexanol and Cyclohexanone, Ullmann's Encyclopedia of Industrial Chemistry*, Wiley-VCH, Weinheim, **2005**.

[15] I. Hermans, J. Peeters, P. A. Jacobs, *Top. Catal.* **2008**, *48*, 41.

[16] W. Bartknecht, *Explosionen – Ablauf und Schutzmassnahmen*, Springer-Verlag, Berlin, **1980**.

[17] K. Nabert, G. Schön, *Sicherheitstechnische Kennzahlen brennbarer Gase und Dämpfe*, 2nd ed., Deutscher Eichverlag, Braunschweig, **1978**.

[18] I. Hermans, P. A. Jacobs, J. Peeters, *ChemPhysChem* **2006**, *7*, 1142.

[19] N. Turrà, U. Neuenschwander, A. Baiker, J. Peeters, I. Hermans, *Chem. Eur. J.* **2010**, *16*, 13226.

[20] E. Spier, U. Neuenschwander, I. Hermans, *Angew. Chem. Int. Ed.* **2013**, *52*, 1581.

[21] F. Minisci, C. Gambarotti, M. Pierini, O. Porta, C. Punta, F. Recupero, M. Lucarini, V. Mugnaini, *Tetrah. Lett.* **2006**, 1421.

[22] F. Minisci, C. Gambarotti, S. Prosperini, N. Pastori, F. Recupero, C. Punta, *Adv. Synth. Catal.* **2011**, *353*, 147.

[23] R. Spaccini, L. Liguori, C. Punta, H.-R. Bjørsvik, *ChemSusChem* **2012**, *5*, 261.

[24] L. Melone, S. Prosperini, C. Gambarotti, N. Pastori, F. Recupero, C. Punta, *J. Mol. Cat. A: Chem.* **2012**, *355*, 155.

[25] A. K. Suresh, T. Sridhar, O. E. Potter, *AIChE J.* **1988**, *34*, 55.

[26] under the assumption that $k_{\text{prop}}^{\text{XH}}[\text{XH}] \gg k_{\text{prop}}^{\text{CyH}}[\text{CyH}]$ and $k_{\text{init}}^{\text{XH}} \gg k_{\text{init}}^{\text{CyH}}$

[27] NIST webbook

[28] J. Chai, M. Head-Gordon, *Phys. Chem. Chem. Phys.* **2008**, *10*, 6615.

[29] K. S. Thanthiriwatte, E. G. Hohenstein, L. A. Burns, C. D. Sherrill, *J. Chem. Theory Comput.* **2011**, *7*, 88.

[30] *Gaussian 09*, Revision A.02, M. J. Frisch, G. W. Trucks, H. B. Schlegel, G. E. Scuseria, M. A. Robb, J. R. Cheeseman, G. Scalmani, V. Barone, B. Mennucci, G. A. Petersson, H. Nakatsuji, M. Caricato, X. Li, H. P. Hratchian, A. F. Izmaylov, J. Bloino, G. Zheng, J. L. Sonnenberg, M. Hada, M. Ehara, K. Toyota, R. Fukuda, J. Hasegawa, M. Ishida, T. Nakajima, Y. Honda, O. Kitao, H. Nakai, T. Vreven, J. A. Montgomery, Jr., J. E. Peralta, F. Ogliaro, M. Bearpark, J. J. Heyd, E. Brothers, K. N. Kudin, V. N. Staroverov, R.

Kobayashi, J. Normand, K. Raghavachari, A. Rendell, J. C. Burant, S. S. Iyengar, J. Tomasi, M. Cossi, N. Rega, J. M. Millam, M. Klene, J. E. Knox, J. B. Cross, V. Bakken, C. Adamo, J. Jaramillo, R. Gomperts, R. E. Stratmann, O. Yazyev, A. J. Austin, R. Cammi, C. Pomelli, J. W. Ochterski, R. L. Martin, K. Morokuma, V. G. Zakrzewski, G. A. Voth, P. Salvador, J. J. Dannenberg, S. Dapprich, A. D. Daniels, Ö. Farkas, J. B. Foresman, J. V. Ortiz, J. Cioslowski, D. J. Fox, Gaussian, Inc., Wallingford CT, **2009**.

[31] See, for example: a) G. Olason, D. C. Sherrington, *React. Funct. Polym.* **1999**, *42*, 163; b) M. Salavati-Niasari, F. Farzaneh, M. Ghandi, *J. Mol. Catal. A* **2002**, *186*, 101; c) A. Chica, G. Gatti, B. Moden, L. Marchese, E. Iglesia, *Chem. Eur. J.* **2006**, *12*, 1960; d) H. E. B. Lempers, R. A. Sheldon, *Stud. Surf. Sci. Catal.* **1997**, *110*, 557, edited by R. K. Grasselli, S. T. Oyama, A. M. Gaffney, J. E. Lyons; e) K. Kervinen, H. Korpi, J. G. Mesu, F. Soulimani, T. Repo, B. Rieger, M. Leskelä, B. M. Weckhuysen, *Eur. J. Inorg. Chem.* **2005**, 2591.

[32] a) S. Tanase, E. Bouwman, J. Reedijk, *Appl. Catal. A* **2004**, *259*, 101; b) R. van Gorkum, E. Bouwman, *Coord. Chem. Rev.* **2005**, *249*, 1709.

[33] a) F. Haber, J. Weiss, *Naturwissenschaften* **1932**, *20*, 948; b) F. Haber, J. Weiss, *Proc. R. Soc. London Ser. A* **1934**, *147*, 332; c) G. Sosnovsky, D. J. Rawlinson, *Organic Peroxides*, *Vol. 2* (Ed.: D. Swern), Wiley, New York, **1971**, p. 153; d) R. A. Sheldon, J. K. Kochi, *Adv. Catal.* **1976**, *25*, 272; e) S. Goldstein, D. Meyerstein, *Acc. Chem. Res.* **1999**, *32*, 547; f) W. H. Koppenol, *Redox Rep.* **2001**, *6*, 229.

[34] G. W. Parshall, S. D. Ittel, *Homogeneous Catalysis: the Applications and Chemistry of Catalysis by Soluble Transition Metal Complexes*, 2nd ed., Wiley, New York, **1992**.

[35] Yu. S. Zimin, E. P. Talzi, V. M. Nekipelov, V. D. Chinakov, K. I. Zamaraev, *React. Kinet. Catal. Lett.* **1985**, *29*, 225.

[36] N. A. Johnson, E. S. Gould, *J. Am. Chem. Soc.* **1973**, *95*, 5198.

[37] a) E. J. Y. Scott, *J. Phys. Chem.* **1970**, *74*, 1174; b) R. Prikryl, A. Tkac, L. Malik, L. Omelka, K. Vesely, *Collect. Czech. Chem. Commun.* **1975**, *40*, 104; c) R. P. Houghton,

C. R. Rice, *Polyhedron* **1996**, *15*, 1893; d) P. G. Harris, R. P. Houghton, P. L. Taylor, *Polyhedron* **1997**, *16*, 2651.

[38] C. A. Tolman, J. D. Druliner, P. J. Krusic, M. J. Nappa, W. C. Seidel, I. D. Williams, S. D. Ittel, *J. Mol. Catal.* **1988**, *48*, 129.

[39] F. Minisci, F. Recupero, G. F. Pedulli, M. Lucarini, *J. Mol. Catal. A* **2003**, *204*, 63.

[40] a) R. A. Sheldon, M. Wallau, I. W. C. E. Arends, U. Schuchardt, *Acc. Chem. Res.* **1998**, *31*, 485; b) R. A. Sheldon, I. W. C. E. Arends, H. E. B. Lempers, *Catal. Today* **1998**, *41*, 387; c) B. Moden, B. Z. Zhan, J. Dakka, J. G. Santiesteban, E. Iglesia, *J. Phys. Chem. C* **2007**, *111*, 1402; d) B. Z. Zhan, B. Moden, J. Dakka, J. G. Santiesteban, E. Iglesia, *J. Catal.* **2007**, *245*, 316; e) B. Moden, B. Z. Zhan, J. Dakka, J. G. Santiesteban, E. Iglesia, *J. Catal.* **2006**, *239*, 390; f) B. Modén, L. Oliviero, J. Dakka, J. G. Santiesteban, E. Iglesia, *J. Phys. Chem. B* **2004**, *108*, 5552; g) F. X. L. i Xamena, O. Casanova, R. G. Tailleur, H. Garcia, A. Corma, *J. Catal.* **2008**, *255*, 220.

[41] a) S. S. Ivanchev, P. I. Selivanov, V. V. Konovalenko, *J. Appl. Spectrosc.* **1975**, *22*, 877; b) O. P. Yablonskii, N. S. Lastochkina, V. A. Belyayev, *Pet. Chem. USSR* **1973**, *13*, 261; O. P. Yablonskii, N. S. Lastochkina, V. A. Belyayev, *Neftekhimiya* **1973**, *13*, 851.

[42] Y. Zhao, D. G. Truhlar, *J. Phys. Chem. A* **2005**, *109*, 4209.

[43] a) A. D. Becke, *J. Chem. Phys.* **1992**, *96*, 2155; A. D. Becke, *J. Chem. Phys.* **1992**, *97*, 9173; A. D. Becke, *J. Chem. Phys.* **1993**, *98*, 5648; b) C. Lee, W. Yang, R. G. Parr, *Phys. Rev. B* **1988**, *37*, 785.

[44] a) J. P. Perdew, *Phys. Rev. B* **1986**, *33*, 8822; b) J. P. Perdew, *Phys. Rev. B* **1986**, *34*, 7046.

[45] M. Weber, H. Fischer, *J. Am. Chem. Soc.* **1999**, *121*, 7381.

[46] K. U. Ingold, *Acc. Chem. Res.* **1969**, *2*, 1.

[47] S. W. Benson, *The Foundations of Chemical Kinetics*, McGraw-Hill, New York, **1960**.

[48] a) E. Rabinowitch, W. C. Wood, *Trans. Faraday Soc.* **1936**, *32*, 547; b) S. Aditya, J. E. Willard, *J. Am. Chem. Soc.* **1957**, *79*, 2680.

[49] R. Hiatt, J. Clipsham, T. Visser, *Can. J. Chem.* **1964**, *42*, 2754.

[50] R. Atkinson, D. L. Baulch, R. A. Cox, R. F. Hampson, J. A. Kerr, M. J. Rossi, J. Troe, *J. Phys. Chem. Ref. Data* **1997**, *26*, 1329.

[51] C. Canepa, M. Mosso, A. Maranzana, G. Tonachini, *Eur. J. Org. Chem.* **2005**, 342.

[52] J. A. Howard, *Peroxyl Radicals* (Ed.: Z. Alfassi), Wiley, New York, **1997**.

[53] J. F. Black, *J. Am. Chem. Soc.* **1978**, *100*, 527.

[54] a) F. A. Chavez, C. V. Nguyen, M. M. Olmstead, P. K. Mascharak, *Inorg. Chem.* **1996**, *35*, 6282; b) F. A. Chavez, P. K. Mascharak, *Acc. Chem. Res.* **2000**, *33*, 539.

[55] *Gaussian 03*, Revision D.01, M. J. Frisch, G. W. Trucks, H. B. Schlegel, G. E. Scuseria, M. A. Robb, J. R. Cheeseman, J. A. Montgomery, Jr., T. Vreven, K. N. Kudin, J. C. Burant, J. M. Millam, S. S. Iyengar, J. Tomasi, V. Barone, B. Mennucci, M. Cossi, G. Scalmani, N. Rega, G. A. Petersson, H. Nakatsuji, M. Hada, M. Ehara, K. Toyota, R. Fukuda, J. Hasegawa, M. Ishida, T. Nakajima, Y. Honda, O. Kitao, H. Nakai, M. Klene, X. Li, J. E. Knox, H. P. Hratchian, J. B. Cross, V. Bakken, C. Adamo, J. Jaramillo, R. Gomperts, R. E. Stratmann, O. Yazyev, A. J. Austin, R. Cammi, C. Pomelli, J. W. Ochterski, P. Y. Ayala, K. Morokuma, G. A. Voth, P. Salvador, J. J. Dannenberg, V. G. Zakrzewski, S. Dapprich, A. D. Daniels, M. C. Strain, O. Farkas, D. K. Malick, A. D. Rabuck, K. Raghavachari, J. B. Foresman, J. V. Ortiz, Q. Cui, A. G. Baboul, S. Clifford, J. Cioslowski, B. B. Stefanov, G. Liu, A. Liashenko, P. Piskorz, I. Komaromi, R. L. Martin, D. J. Fox, T. Keith, M. A. Al-Laham, C. Y. Peng, A. Nanayakkara, M. Challacombe, P. M. W. Gill, B. Johnson, W. Chen, M. W. Wong, C. Gonzalez, J. A. Pople, Gaussian, Inc., Wallingford CT, **2004**.

[56] N. M. Emanuel, Z. K. Maizus, I. P. Skibida, *Angew. Chem. Int. Ed Engl.* **1969**, *8*, 97.

[57] D. L. Vanoppen, D. E. De Vos, M. J. Genet, P. G. Rouxhet, P. A. Jacobs, *Angew. Chem. Int. Ed. Engl.* **1995**, *34*, 560.

[58] M. Nowotny, L. N. Pedersen, U. Hanefeld, T. Maschmeyer, *Chem. Eur. J.* **2002**, *8*, 3724.

[59] A. Ramanathan, M. S. Hamdy, R. Parton, T. Maschmeyer, J. C. Jansen, U. Hanefeld, *Appl. Catal. A Gen.* **2009**, *355*, 78.

[60] G. Sankar, R. Raja, J. M. Thomas, *Catal. Lett.* **1998**, *55(1)*, 15.

[61] E. Breynaert, I. Hermans, B. Lambie, G. Maes, J. Peeters, A. Maes, P. A. Jacobs, *Angew. Chem. Int. Ed.* **2006**, *45*, 7584.

[62] I. Hermans, E. Breynaert, H. Poelman, R. De Gryse, D. Liang, G. Van Tendeloo, A. Maes, J. Peeters, P. A. Jacobs, *Phys. Chem. Chem. Phys.* **2007**, *9*, 5382.

[63] R. Strobel, A. Baiker, S. E. Pratsinis, *Adv. Power Technol.* **2006**, *17*, 457.

[64] R. Strobel, S. E. Pratsinis, *J. Mater. Chem.* **2007**, *17*, 4743.

[65] R. Mueller, L. Madler, S. E. Pratsinis, *Chem. Eng. Sci.* **2003**, *58*, 1969.

[66] L. Madler, H. K. Kammler, R. Mueller, S. E. Pratsinis, *Aerosol Sci.* **2002**, *33*, 369.

[67] B. Schimmoeller, H. Schulz, A. Ritter, A. Reitzmann, B. Kraushaar-Czarnetzki, A. Baiker, S. E. Pratsinis, *J. Catal.* **2008**, *256*, 74.

[68] B. Schimmoeller, F. Hoxha, T. Mallat, F. Krumeich, S. E. Pratsinis, A. Baiker, *Appl. Catal. A Gen.* **2010**, *374*, 48.

[69] R. Wengeler, A. Teleki, M. Vetter, S. E. Pratsinis, H. Nirschl, *Langmuir* **2006**, *22*, 4928.

[70] A. Camenzind, H. Schulz, A. Teleki, G. Beaucage, T. Narayanan, S. E. Pratsinis, *Eur. J. Inorg. Chem.* **2008**, *6*, 911.

[71] B. Schimmoeller, Y. J. Jiang, S. E. Pratsinis, A. Baiker, *J. Catal.* **2010**, *274*, 64.

[72] H. Schulz, L. Madler, S. E. Pratsinis, N. Moszner, *Adv. Funct. Mater.* **2005**, *15*, 830.

[73] T. Tani, L. Madler, S. E. Pratsinis, *J. Mater. Sci.* **2002**, *37*, 4627.

[74] J. H. Ashley, P. C. H. Mitchell, *J. Chem. Soc.* **1968**, 2821.

[75] A. A. Verberckmoes, B. M. Weckhuysen, R. A. Schoonheydt, *Microporous Mesoporous Mater.* **1998**, *22*, 165.

[76] B. M. Weckhuysen, R. R. Rao, J. A. Martens, R. A. Schoonheydt, *Eur. J. Inorg. Chem.* **1999**, 565.

[77] B. M. Weckhuysen, R. A. Schoonheydt, *Spectroscopy of transition metal ions on surfaces* (Eds.: B. M. Weckhuysen, P. Van Der Voort, G. Catana), Leuven University Press, Leuven, **2000**.

[78] I. Hermans, J. Peeters, P. A. Jacobs, *J. Phys. Chem. A* **2008**, *112*, 1747.

[79] B. P. C. Hereijgers, B. M. Weckhuysen, *J. Catal.* **2010**, *270*, 16.

List of Abbreviations and Acronyms

6-31G (and similar)	Pople split-valence basis set
ATR	attenuated total reflectance
BET	Brunauer-Emmett-Teller
CPC	column precipitation chromatography
DFT	density functional theory
DRIFT	diffuse reflectance infrared Fourier transform
DRS	diffuse reflectance spectroscopy
FID	flame ionization detector
FSP	flame spray pyrolysis
GC	gas chromatography
ICP-OES	inductively coupled plasma – optical emission spectrometer
IR	infrared
LANL2DZ	Los Alamos effective core potential
MS	mass spectrometry
PES	potential energy surface
QSS	quasi steady state
TPD	temperature programmed desorption
TS	transition state
TST	transition state theory
UB3LYP	unrestricted Becke-Lee-Yang-Parr hybrid functional

UBP86	unrestricted Becke-Perdew hybrid funtional
UCCSD(T)	unrestricted coupled cluster, using single and double substitutions, non-iteratively including triple exitations
UV/Vis	ultraviolet/visible light
ZPE	zero point energy

acac	acetylacetonate
MSTFA	*N*-methyl-*N*-(trimethylsilyl)trifluoroacetamide
PEEK	Polyether Ether Ketone
SS316	stainless steel (containing 16% Cr, 10% Ni, 2% Mo)

λ	wavelength; for UV/Vis usually in nm (greek lambda)
μ	bridging properties of ligands (greek mu)
ν	chain length (greek nu)
τ	characteristic lifetime, also half-life (greek tau)

Q=O	ketone (or also aldehyde), *e.g.*, cyclohexanone
$R^{\bullet}$ (*e.g.*, $Cy^{\bullet}$)	alkyl radical (*e.g.*, cyclohexyl radical)
RH; *e.g.*, CyH	hydrocarbon substrate (with a C-H bond); *e.g.*, cyclohexane
$RO^{\bullet}$ (*e.g.*, $CyO^{\bullet}$)	alkoxyl radical (*e.g.*, cyclohexyl oxyl radical)
ROH; *e.g.*, CyOH	alcohol; *e.g.*, cyclohexanol
$ROO^{\bullet}$ (*e.g.*, $CyOO^{\bullet}$)	peroxyl radical (*e.g.*, cyclohexyl peroxyl radical)
ROOH; *e.g.*, CyOOH	hydroperoxide; *e.g.*, cyclohexyl hydroperoxide
$R_{-\alpha H}{}^{\bullet}OOH$	radical resulting upon abstraction of an αH-atom from ROOH

List of Publications

Publications in Connection with this Thesis

- „Molecule-Induced Peroxide Homolysis“
  N. Turrà, U. Neuenschwander, I. Hermans
  submitted
  (chapter 3)

- “Aerobic Oxidation of Cyclohexane Catalyzed by Flame-Made Nano-Structured Co/SiO_2 Materials”
  N. Turrà, A. Blanco Acuña, B. Schimmöller, B. Mayr-Schmölzer, P. Mania, I. Hermans
  Top. Catal. **2011**, *54*, 737.
  (chapters 2 and 5)

- “Mechanism of the Catalytic Deperoxidation of *tert*-Butyl Hydroperoxide with $Co(acac)_2$“
  N. Turrà, U. Neuenschwander, A. Baiker, J. Peeters, I. Hermans
  Chem. Eur. J. **2010**, *16*, 13226.
  (chapter 4)

- „Understanding Selective Oxidations“
  U. Neuenschwander, N. Turrà, C. Aellig, P. Mania, I. Hermans
  CHIMIA **2010**, *64*, 225.
  (chapter 1)

Other Publications

- „Selective Oxidation Catalysis: Opportunities and Challenges“
  I. Hermans, E. S. Spier, U. Neuenschwander, N. Turrà, A. Baiker
  Top. Catal. **2009**, *52*, 1162.

Conferences

- N. Turrà, U. Neuenschwander, I. Hermans
  „Understanding the Homolytic Activation of Alkyl Peroxides by Homogeneous and Heterogeneous Cobalt Catalysts”
  SCS Fall Meeting (Zurich, Switzerland), September 2012

- N. Turrà, U. Neuenschwander, I. Hermans
  „Understanding the Homolytic Activation of Peroxides by Homogeneous and Heterogeneous Cobalt Catalysts”
  15th International Congress on Catalysis (Munich, Germany), July 2012

- I. Hermans, E. S. Spier, U. Neuenschwander, N. Turrà, A. Baiker
  Abs. Pap. Am. Chem. Soc. **2009**, *238*, 22-CATL.
  „Selective Oxidation Catalysis: Opportunities and Challenges“
  238th ACS Fall Meeting (Washington, USA), August 2009